Quasi-3D Beam Models for the Computation of Eigenfrequencies of Functionally Graded Beams with Arbitrary Boundary Conditions

Fiorenzo A. Fazzolari[1,*]

University of Cambridge, Department of Engineering, Trumpington Street, Cambridge, CB2 1PZ, UK

Abstract

The present article deals with the free vibration analysis of three-dimensional metallic and functionally graded beams with arbitrary boundary conditions. The investigation is carried out by using refined variable-kinematics quasi-3D beam theories. The latter are hierarchically generated by using the method of power series expansion of displacement components. In this respect, each displacement variable, in the displacement field, can be expanded at any desired order, independently from the others and regarding to the results accuracy and the computational cost. The weak-form of the governing equations is derived via the Principle of the Virtual Displacements (PVD), while the Ritz method is used as solution technique. Algebraic Ritz functions, orthogonalised by using the Gram-Schmidt process, are employed in the analysis. Convergence and accuracy of the proposed formulation have been thoroughly examined and commented. A comprehensive assessment of the developed beam models is also provided. The effect of significant parameters such as length-to-thickness ratio (slenderness ratio), volume fraction index, materials and boundary conditions, on the natural frequencies and mode shapes, is discussed.

Keywords: Quasi-3D beam theories, Free vibration, FG beams, Ritz method, Gram-Schmidt process.

*Corresponding author: Tel:+44 1223 (7) 48522
Email address: ff305@cam.ac.uk (Fiorenzo A. Fazzolari)
[1]Research Group: Applied Mechanics;
Academic Division: Mechanics, Materials and Design

1. Introduction

Due to their high versatility beam structures are extensively used in aerospace, civil, ship and mechanical applications, amongst others. In particular, the beam structural element allows the modelling of crucial structural components such as aircraft wing spars, helicopter rotor blades, robot harms as well as concrete and metal/composite constructions in civil and ship engineering, respectively.

During the century many efforts have been focused on the development of axiomatic and asymptotic beam models able to accurately describe the kinematics, and more generally, the mechanical behaviour of beam structures, some of them can be found in Refs. [1–8]. Recently some interesting beam formulations have been provided by Yu, Hodges and co-authors [9–11]. They proposed the variational asymptotic method which led to the computer program variational asymptotic beam sectional analysis (VABS), which has been successfully used for several structural problems. Advanced hierarchical beam models have been developed by Carrera [12], within the framework of Carrera's Unified Formulation (CUF), and are usually referred to as 1D CUF models. The radial basis function (RBF)-pseudospectral method has been employed by Ferreira and Fasshauer [13] for the computation of natural frequencies of shear deformable beams and plates. Exact beam formulations based on the dynamic stiffness method (DSM) have been proposed by Banerjee and co-authors [14–16].

The enhancement in the development of the structural beam models went hand-in-hand with the improvement in the mechanical as well as thermal performances of new advanced materials. Amongst the latter, the Functionally Graded Materials (FGMs) have raised a lot of interest in the research community in the last decade. They showed some outstanding properties, which, in several applications, make them more attractive than classical fibre-reinforced composites. They have turned out to be more advantageous, indeed problems such as delamination, fibre failure, adverse hygroscopic effects etc, are effectively eliminated or non-existent. Thus, due to their potential application in several fields, there is the need to fully understand their mechanical and thermal behaviour.

In this respect, many scientific articles have been recently published on the static and dynamic analysis of FG beams. In particular, Vo *et al.* [17] coped with the static and vibration analysis of FG beams using refined shear deformation theories. Thai and Vo [18] dealt with bending and free vibration analysis of FG beams considering various boundary conditions and shear deformation beam theories. Fundamental frequencies of FG beams using different

high-order beam theories have been provided by Sismek [19]. The same author [20] studied the free and forced vibration behaviour of bi-directional functionally graded materials (BD-FGMs) of Timoshenko beams with various boundary conditions. Chunhua and Wang [21] provided and accurate free vibration analysis of Euler-type FG beams by using the weak-form quadrature element method. Wang *et al.* [22] analysed the free vibration behaviour of two-directional FG beams. Lü *et al.* [23] proposed semi-analytical elasticity solutions for bi-directional functionally graded beams. Alshorbagy *et al.* [24] studied the free vibration characteristics of a functionally graded beam by using FEM formulation. Maganti and Nullari [25] investigated the free vibration analysis of pre-twisted rotating FG beams by using Rayleigh–Ritz method. The same authors [26] studied the flapwise bending vibration analysis of functionally graded rotating double-tapered beams. Free vibration of FG Timoshenko beams with through-width delamination have been investigated by Li and Fan [27]. Ke *et al.* [28] coped with the non-linear vibration of edged cracked FG beams using differential quadrature method and Timoshenko beam model. Vibration characteristics of stepped beams made of FGM using differential transformation method were analysed by Wattanasakulpong and Charoensuk [29]. The same authors [30] proposed the study of flexural vibration of imperfect FG beams based on Timoshenko beam theory and Chebyshev collocation method. Shegokar and Lal [31] coped with a stochastic finite element non-linear free vibration analysis of piezoelectric FG beams subjected to thermo-piezoelectric loadings with material uncertainties. Nonlinear forced vibration analysis of clamped functionally graded beams have been analysed by Shooshtari and Rafiee [32]. A combined Fourier series – Galerkin method for the analysis of FG beams have been proposed by Zhu and Sankar [33]. Azadi [34] dealt with the free and forced vibration analysis of FG beam considering temperature dependency of material properties. Pradhan and Chackraverty [35] investigated the effects of different shear deformation theories on the free vibration of functionally graded beams. Librescu *et al.* [36] investigated the free vibration and stability behaviour of thin walled beams made of FGMs and operating in high temperature environment. Giunta *et al.* [37] proposed hierarchical beam theories for an accurate free vibration analysis of functionally graded beams. The same authors [38] coped with a thermo-mechanical analysis of FG beams via hierarchical modelling. Su and Benerjee [15] proposed a development of dynamic stiffness method for the free vibration analysis of FG Timoshenko beams. Ziane *et al.* [39] coped with tree vibration analysis of thin and thick-walled FGM box beams by using an exact dynamic stiffness

matrix on the basis of first-order shear deformation theory. Xu *et al.* [40] investigated the stochastic dynamic characteristics of FGM beams with random material properties. Eroglu [41] proposed a study on in-plane free vibrations of circular beams made of FGM in thermal environment. Roque and Martins [42] used the RBF numerical method combined with the differential evolution for optimization of FG beams. Free vibrations of FG spatial curved beams have been analysed by Yousefi and Rastgoo [43]. FGM structures have been widely analysed for free vibration problems by Tornabene *et al.* [44–46]. In the latter the attention has been primarily focused on FGM doubly-curved shells with variable radii of curvature. An extensive contribution in the thermo-mechanical analysis of FG beams has been provided by Batra *et al.* [47, 48].

In the present article the Hierarchical Ritz Formulation (HRF), extensively employed in the analysis of laminated composite plates and shells [49–59] has been extended to the free vibration analysis of metallic and FG beams with general boundary conditions. Advanced and refined beam models with hierarchical capabilities have been employed and assessed by comparison with 3D FEM solutions provided by using commercial FEM software such as ABAQUS [60] and ANSYS [61], as well as other results available in literature. The proposed formulation has an intrinsic capability of dealing with more general structural configurations. Then, although the analysis has been restricted to FG beams with rectangular cross-section, more complex geometries accounting for various cross-sections or tapered shapes, can be investigated with no substantial changes in the theoretical development.

Moreover, the developed formulation represents a particular case of what in a more general sense is known as axiomatic/asymptotic method (AAM), and is here based on 1×1 secondary fundamental nuclei. More specifically, the complete 3×3 primary fundamental nucleus is composed by nine secondary nuclei six of which are independent. Each single secondary nucleus is expanded independently from the others and according to the selected beam theory. Once all of the secondary nuclei have been expanded separately, they are then assembled in the final primary nucleus. The conceptual procedure is essentially the same for plates and shells. More information about the assembly procedure can be found in a previous author's article [55]. For the sake of completeness it must be said that the formulation based on 1×1 nuclei was first developed for plate and named Generalized Unified Formulation (GUF) [62–64].

The analysis is performed by using algebraic Ritz functions orthogonalized via the Gram-

Smidth process. Convergence and accuracy of the presented formulation have been extensively examined in two proposed case-studies. Results have been presented in terms of natural frequencies and mode shapes. The effect of significant parameters such as length-to-thickness ratio (slenderness ratio), volume fraction index, materials and boundary conditions, has been discussed.

2. Geometric and Constitutive relations

The geometrical features of the beam structures studied in this article are shown in Fig. 1. In particular, the cross-section area lying in the plane (xy) is named Ω and the axial coordinate z is referred to as reference line of the beam. In the case of FG beams (see Fig. 2), the gradation is considered in the beam-thickness direction. The symbols b and h denote the beam width and thickness, respectively. According to the reference system the notation for the displacement vector is:

$$\mathbf{u}\left(x,y,z,t\right)=\left[\begin{array}{ccc} u_x\left(x,y,z,t\right) & u_y\left(x,y,z,t\right) & u_z\left(x,y,z,t\right) \end{array}\right]^T \tag{1}$$

Superscript T represents the transposition operator. The stresses, $\boldsymbol{\sigma}$, and the strains, $\boldsymbol{\varepsilon}$, are grouped as follows:

$$\boldsymbol{\sigma}_{pH}=\left\{\begin{array}{c}\sigma_{xx}\\ \sigma_{yy}\\ \tau_{xy}\end{array}\right\},\quad \boldsymbol{\sigma}_{nH}=\left\{\begin{array}{c}\tau_{xz}\\ \tau_{yz}\\ \sigma_{zz}\end{array}\right\},\quad \boldsymbol{\varepsilon}_{pG}=\left\{\begin{array}{c}\varepsilon_{xx}\\ \varepsilon_{yy}\\ \gamma_{xy}\end{array}\right\},\quad \boldsymbol{\varepsilon}_{nG}=\left\{\begin{array}{c}\gamma_{xz}\\ \gamma_{yz}\\ \varepsilon_{zz}\end{array}\right\} \tag{2}$$

The subscripts n and p denote out-of-plane and in-plane components, respectively, whilst the subscript H and G state that Hooke's law and geometric relations are used. The strain-displacement relations are

$$\begin{aligned}\boldsymbol{\varepsilon}_{pG}&=\mathbf{D}_p\mathbf{u}\\ \boldsymbol{\varepsilon}_{nG}&=\mathbf{D}_n\mathbf{u}=\left(\mathbf{D}_{np}+\mathbf{D}_{nz}\right)\mathbf{u}\end{aligned} \tag{3}$$

where $\mathbf{D}_p$, $\mathbf{D}_n$, $\mathbf{D}_{np}$ and $\mathbf{D}_{nz}$ are differential matrix operators defined as follows

$$\begin{aligned}\mathbf{D}_p&=\left[\begin{array}{ccc}\frac{\partial}{\partial x}&0&0\\0&\frac{\partial}{\partial y}&0\\\frac{\partial}{\partial y}&\frac{\partial}{\partial x}&0\end{array}\right],\qquad \mathbf{D}_n=\left[\begin{array}{ccc}\frac{\partial}{\partial z}&0&\frac{\partial}{\partial x}\\0&\frac{\partial}{\partial z}&\frac{\partial}{\partial y}\\0&0&\frac{\partial}{\partial z}\end{array}\right],\\ \mathbf{D}_{np}&=\left[\begin{array}{ccc}0&0&\frac{\partial}{\partial x}\\0&0&\frac{\partial}{\partial y}\\0&0&0\end{array}\right],\qquad \mathbf{D}_{nz}=\left[\begin{array}{ccc}\frac{\partial}{\partial z}&0&0\\0&\frac{\partial}{\partial z}&0\\0&0&\frac{\partial}{\partial z}\end{array}\right]\end{aligned} \tag{4}$$

The 3D constitutive equations according to Hooke's law are given as

$$\boldsymbol{\sigma} = \mathbf{C}\boldsymbol{\varepsilon} \tag{5}$$

By using Eq. (2), the previous equation becomes

$$\begin{aligned} \boldsymbol{\sigma}_{pH} &= \mathbf{C}_{pp}\,\boldsymbol{\varepsilon}_{pG} + \mathbf{C}_{pn}\,\boldsymbol{\varepsilon}_{nG} \\ \boldsymbol{\sigma}_{nH} &= \mathbf{C}_{np}\,\boldsymbol{\varepsilon}_{pG} + \mathbf{C}_{nn}\,\boldsymbol{\varepsilon}_{nG} \end{aligned} \tag{6}$$

where matrices $\mathbf{C}_{pp}$, $\mathbf{C}_{nn}$, $\mathbf{C}_{pn}$ and $\mathbf{C}_{np}$ are:

$$\begin{aligned} \mathbf{C}_{pp} &= \begin{bmatrix} C_{11} & C_{12} & C_{16} \\ C_{12} & C_{22} & C_{26} \\ C_{16} & C_{26} & C_{66} \end{bmatrix}, \quad \mathbf{C}_{nn} = \begin{bmatrix} C_{55} & C_{45} & 0 \\ C_{45} & C_{44} & 0 \\ 0 & 0 & C_{33} \end{bmatrix}, \\ \mathbf{C}_{pn} &= \begin{bmatrix} 0 & 0 & C_{13} \\ 0 & 0 & C_{23} \\ 0 & 0 & C_{36} \end{bmatrix}, \qquad \mathbf{C}_{np} = \begin{bmatrix} 0 & 0 & 0 \\ 0 & 0 & 0 \\ C_{13} & C_{23} & C_{36} \end{bmatrix} \end{aligned} \tag{7}$$

In the case of metallic beams the elastic coefficients C_{ij} become

$$\begin{cases} C_{11} = C_{22} = C_{33} = \dfrac{(1-\nu)\,E}{(1+\nu)\,(1-2\,\nu)} = \lambda + 2\,G \\ C_{12} = C_{13} = C_{23} = \dfrac{\nu\,E}{(1+\nu)\,(1-2\,\nu)} = \lambda \\ C_{44} = C_{55} = C_{66} = \dfrac{E}{2\,(1+\nu)} = \mu = G \end{cases} \tag{8}$$

where λ and μ are the Lamé coefficients, and G is the shear modulus.

2.1. One-directional functionally graded beams

In the case of one-directional FG beams, the 3D constitutive equations are given as

$$\boldsymbol{\sigma} = \mathbf{C}\,(x)\,\boldsymbol{\varepsilon} \tag{9}$$

being x the beam-thickness coordinate. By using Eq. (2), the previous equation becomes

$$\begin{aligned} \boldsymbol{\sigma}_{pH} &= \mathbf{C}_{pp}\,(x)\;\boldsymbol{\varepsilon}_{pG} + \mathbf{C}_{pn}\,(x)\;\boldsymbol{\varepsilon}_{nG} \\ \boldsymbol{\sigma}_{nH} &= \mathbf{C}_{np}\,(x)\;\boldsymbol{\varepsilon}_{pG} + \mathbf{C}_{nn}\,(x)\;\boldsymbol{\varepsilon}_{nG} \end{aligned} \tag{10}$$

where matrices $\mathbf{C}_{pp}(x)$, $\mathbf{C}_{nn}(x)$, $\mathbf{C}_{pn}(x)$ and $\mathbf{C}_{np}(x)$ are:

$$\mathbf{C}_{pp}(x) = \begin{bmatrix} C_{11}(x) & C_{12}(x) & 0 \\ C_{12}(x) & C_{22}(x) & 0 \\ 0 & 0 & C_{66}(x) \end{bmatrix}, \quad \mathbf{C}_{nn}(x) = \begin{bmatrix} C_{55}(x) & 0 & 0 \\ 0 & C_{44}(x) & 0 \\ 0 & 0 & C_{33}(x) \end{bmatrix},$$
$$\mathbf{C}_{pn}(x) = \begin{bmatrix} 0 & 0 & C_{13}(x) \\ 0 & 0 & C_{23}(x) \\ 0 & 0 & 0 \end{bmatrix}, \qquad \mathbf{C}_{np}(x) = \begin{bmatrix} 0 & 0 & 0 \\ 0 & 0 & 0 \\ C_{13}(x) & C_{23}(x) & 0 \end{bmatrix} \tag{11}$$

The volume fraction of the ceramic phase is defined according to the following power-law (see Fig. 3)

$$V_c(x) = \left(\frac{1}{2} + \frac{x}{h}\right)^p \qquad x \in \left[-\frac{h}{2}, \frac{h}{2}\right] \tag{12}$$

where h is the thickness of the beam and the exponent p is the volume fraction index indicating the material variation through the thickness direction. The volume fraction of the metal phase is give as $V_m(x) = 1 - V_c(x)$. Young's modulus E, Poisson's coefficient ν and density ρ are computed by the law-of-mixtures

$$\begin{cases} E(x) = (E_c - E_m)\, V_c(x) + E_m \\ \nu(x) = (\nu_c - \nu_m)\, V_c(x) + \nu_m \\ \rho(x) = (\rho_c - \rho_m)\, V_c(x) + \rho_m \end{cases} \tag{13}$$

Finally the effective FG material coefficients $C_{ij}(x)$, derived after careful considerations based on micro-mechanical approaches, are given as follows

$$\begin{cases} C_{11}(x) = C_{22}(x) = C_{33}(x) = \dfrac{E(x)\left\{1 - [\nu(x)]^2\right\}}{1 - 3[\nu(x)]^2 - 2[\nu(x)]^3} \\ C_{12}(x) = C_{13}(x) = C_{23}(x) = \dfrac{E(x)\left\{\nu(x) - [\nu(x)]^2\right\}}{1 - 3[\nu(x)]^2 - 2[\nu(x)]^3} \\ C_{44}(x) = C_{55}(x) = C_{66}(x) = \dfrac{E(x)}{2[1 + \nu(x)]} \end{cases} \tag{14}$$

3. Variable-Kinematics beam theories

The proposed hierarchical beam theories are generated on the basis of axiomatic assumptions. The latter are focused on the reduction of the 3D elastic problem in 2D (plate/shell structures) or 1D (beam structures). This simplification reduces significantly the complexity

of the studied problems while retaining all the most important physical features which characterize the phenomenon itself. The simplest beam theory based on axiomatic assumptions was proposed by Euler [1] and it is usually referred to as Euler-Bernoulli beam theory (EBBT). The displacement field associated with the hypothesis of the EBBT is given as follows

$$\begin{aligned} u_x &= u_{x_1} \\ u_y &= u_{y_1} \\ u_z &= u_{z_1} + x\frac{\partial u_{y_1}}{\partial x} + y\frac{\partial u_{z_1}}{\partial y} \end{aligned} \tag{15}$$

In this theory, both transverse shear strains and transverse normal strain are discarded, being in classical applications negligible with respect to the in-plane ones. The inclusion of transverse shear strains, in the above-mentioned beam model, leads to Timoshenko beam theory (TBT) [2]

$$\begin{aligned} u_x &= u_{x_1} \\ u_y &= u_{y_1} \\ u_z &= u_{z_1} + x\,\theta + y\,\phi \end{aligned} \tag{16}$$

The development of higher order beam theories allows more generally a more accurate description of the beam kinematics, which is needed above all in unconventional structural mechanics applications such as static and dynamic analysis of beams subjected to multifield loadings. The complications which rise when dealing with these problems make meaningless the use of classical beam theories, EBBT and TBT.

Moreover, the employment of higher order beam theories yields a more accurate modelling of classical beam problems which involve both in and out-of-plane cross-section deformation, torsional mechanics and eventually coupling of the spatial directions. The proposed advanced computational technique is able to generate a class of beam theories in a systematic way. In particular, each displacement variable in the displacement field is expanded at any desired order independently from the others and regarding to the results accuracy and the computational cost. Such artifice becomes extremely useful when multi-field/multi-physics problems, such as thermoelastic and piezoelectric applications [52, 65], are investigated . Thereby, the most general displacement field can be written as follows

$$\begin{aligned} u_x(x,y,z,t) &= F_{\tau_{u_x}}(x,y)\; u_{x\tau_{u_x}}(z,t), \qquad \tau_{u_x} = 0,1,\cdots,N_{u_x} \\ u_y(x,y,z,t) &= F_{\tau_{u_y}}(x,y)\; u_{y\tau_{u_y}}(z,t), \qquad \tau_{u_y} = 0,1,\cdots,N_{u_y} \\ u_z(x,y,z,t) &= F_{\tau_{u_z}}(x,y)\; u_{z\tau_{u_z}}(z,t), \qquad \tau_{u_z} = 0,1,\cdots,N_{u_z} \end{aligned} \tag{17}$$

or in compact form

$$\mathbf{u}\left(x,y,z,t\right)=\mathbf{F}_{\tau}\left(x,y\right)\mathbf{u}_{\tau}\left(z,t\right) \tag{18}$$

where

$$\mathbf{u}_{\tau}\left(z,t\right)=\left\{\begin{array}{c} u_{x\tau_{u_x}}\left(z,t\right) \\ u_{y\tau_{u_y}}\left(z,t\right) \\ u_{z\tau_{u_z}}\left(z,t\right) \end{array}\right\},\quad \mathbf{F}_{\tau}\left(x,y\right)=\left[\begin{array}{ccc} F_{\tau_{u_x}}\left(x,y\right) & 0 & 0 \\ 0 & F_{\tau_{u_y}}\left(x,y\right) & 0 \\ 0 & 0 & F_{\tau_{u_z}}\left(x,y\right) \end{array}\right] \tag{19}$$

$F_{\tau_{u_x}}$, $F_{\tau_{u_y}}$, $F_{\tau_{u_z}}$ are the cross-section functions; $u_{x\tau_{u_x}}$, $u_{y\tau_{u_y}}$, $u_{z\tau_{u_z}}$ are the displacement vector components and N_{u_x}, N_{u_y} and N_{u_z} are the orders of expansion. According to Einstein's notation, the repeated subscripts τ_{u_x}, τ_{u_y}, τ_{u_z} indicate summation.

When the cross-section functions are chosen to be Taylor's series expansion then Eq. (17) can be rewritten as

$$\begin{aligned} u_x\left(x,y,z,t\right)&=\sum_{n_{u_x}=0}^{N_{u_x}}\left[\sum_{n_{u_x}^*=0}^{n_{u_x}} x^{\left(n_{u_x}-n_{u_x}^*\right)}y^{n_{u_x}^*}u_{x_{\tilde{N}_{u_x}}}\left(z,t\right)\right] \\ u_y\left(x,y,z,t\right)&=\sum_{n_{u_y}=0}^{N_{u_y}}\left[\sum_{n_{u_y}^*=0}^{n_{u_y}} x^{\left(n_{u_y}-n_{u_y}^*\right)}y^{n_{u_y}^*}u_{y_{\tilde{N}_{u_y}}}\left(z,t\right)\right] \\ u_z\left(x,y,z,t\right)&=\sum_{n_{u_z}=0}^{N_{u_z}}\left[\sum_{n_{u_z}^*=0}^{n_{u_z}} x^{\left(n_{u_z}-n_{u_z}^*\right)}y^{n_{u_z}^*}u_{z_{\tilde{N}_{u_z}}}\left(z,t\right)\right] \end{aligned} \tag{20}$$

where $\tilde{N}_u=\frac{\left[n_u\left(n_u+1\right)+2\left(n_u^*+1\right)\right]}{2}$. Equation (20) can alternatively be formulated as follows

$$\begin{aligned} u_x&=u_{x_1}+xu_{x_2}+yu_{x_3}+\cdots+x^{N_{u_x}}u_{x_{\frac{\left(N_{u_x}^2+N_{u_x}+2\right)}{2}}}+\cdots+y^{N_{u_x}}u_{x_{N_{u_x}^*}} \\ u_y&=u_{y_1}+xu_{y_2}+yu_{y_3}+\cdots+x^{N_{u_y}}u_{y_{\frac{\left(N_{u_y}^2+N_{u_y}+2\right)}{2}}}+\cdots+y^{N_{u_y}}u_{y_{N_{u_y}^*}} \\ u_z&=u_{z_1}+xu_{z_2}+yu_{z_3}+\cdots+x^{N_{u_z}}u_{z_{\frac{\left(N_{u_z}^2+N_{u_z}+2\right)}{2}}}+\cdots+y^{N_{u_z}}u_{z_{N_{u_z}^*}} \end{aligned} \tag{21}$$

the total number of unknowns for each displacement component is indicated as N_u^*. The latter along with the cross-section functions F_{τ} are related to N_u by means of the Pascal's triangle, which is provided in Tab. 1. The orders N_{u_x}, N_{u_y} and N_{u_z} of the expansion are arbitrary and represent an analysis input. An example of a possible displacement field according to the present approach and by using expansion orders $N_{u_x}=2$, $N_{u_y}=3$ and $N_{u_z}=1$ is given in Eq. (22) as follows

$$\begin{aligned} u_x&=u_{x_1}+xu_{x_2}+yu_{x_3}+x^2u_{x_4}+xyu_{x_5}+y^2u_{x_6} \\ u_y&=u_{y_1}+xu_{y_2}+yu_{y_3}+x^2u_{y_4}+xyu_{y_5}+y^2u_{y_6}+x^3u_{y_7}+x^2yu_{y_8}+xy^2u_{y_9}+y^3u_{y_{10}} \\ u_z&=u_{z_1}+xu_{z_2}+yu_{z_3} \end{aligned} \tag{22}$$

4. Theoretical Formulation

In the derivation of what follows the Principle of Virtual Displacements (PVD) is employed to derive the Hierarchical Ritz Formulation (HRF). The PVD variational statement can be written in its classical form as

$$\delta L_{int} = \delta L_{ext} - \delta L_{ine} \tag{23}$$

where δL_{int}, δL_{ext} and δL_{ine} are the virtual internal work, the virtual external work and the virtual inertial work, respectively. Equation (23) can also be written in a more convenient way as

$$\int_\Omega \int_l \left(\delta \boldsymbol{\varepsilon}_{pG}^T \boldsymbol{\sigma}_{pC} + \delta \boldsymbol{\varepsilon}_{nG}^T \boldsymbol{\sigma}_{nC} \right) \mathrm{d}\Omega \, \mathrm{d}z = \delta L_{ext} - \int_\Omega \int_l \rho \, \delta \mathbf{u} \, \ddot{\mathbf{u}} \, \mathrm{d}\Omega \, \mathrm{d}z \tag{24}$$

When dealing with dynamics problems, Hamilton's principle can also be alternatively used. The latter can be expressed as

$$\int_{t_1}^{t^2} \delta \mathcal{L} \, \mathrm{d}t = 0 \tag{25}$$

where t_1 and t_2 are the initial and the generic instant of time; $\mathcal{L}$ is the Lagrangian which assumes the following form

$$\mathcal{L} = T - \Pi, \quad \text{with} \quad \Pi = U + V \tag{26}$$

T is the kinetic energy and Π is the total potential energy of the system; U and V are the potential strain energy and the potential energy due to the external forces, respectively. The PVD can easily be derived by Hamilton's principle (for more details refer to Section 4.1 of Ref. [52]), and indeed the following relations hold

$$\delta L_{int} = \delta U, \quad \delta L_{ext} = -\delta V, \quad \delta L_{ine} = -\delta T \tag{27}$$

4.1. The Hierarchical Ritz Formulation

In the Ritz method the displacement amplitude vector components $u_{x_{\tau_{u_x}}}$, $u_{y_{\tau_{u_y}}}$ and $u_{z_{\tau_{u_z}}}$ are expressed in series expansion as follows

$$\begin{aligned}
u_{x_{\tau_{u_x}}}(z,t) &= \sum_i^{\mathcal{N}} U_{x\tau_{u_x} i} \, \psi_{x_i}(z) \, e^{\imath \omega_{ij} t} \\
u_{y_{\tau_{u_y}}}(z,t) &= \sum_i^{\mathcal{N}} U_{y\tau_{u_y} i} \, \psi_{y_i}(z) \, e^{\imath \omega_{ij} t} \\
u_{z_{\tau_{u_z}}}(z,t) &= \sum_i^{\mathcal{N}} U_{z\tau_{u_z} i} \, \psi_{z_i}(z) \, e^{\imath \omega_{ij} t}
\end{aligned} \tag{28}$$

where $\imath = \sqrt{-1}$, t is the time and ω_{ij} the circular frequency; $\mathcal{N}$ indicates the order of expansion in the approximation; $U_{x\tau_{u_x}i}$, $U_{y\tau_{u_y}i}$, $U_{z\tau_{u_z}i}$ are the unknown coefficients and ψ_{x_i}, ψ_{y_i}, ψ_{z_i} are the Ritz functions appropriately selected with respect to the features of the problem under investigation. Convergence to the exact solution is guaranteed if the Ritz functions (also known as basis functions) are admissible functions in the used variational principle [49, 50, 66, 67]. The displacement field is then given as

$$\begin{aligned} u_x(x,y,z,t) &= \sum_i^{\mathcal{N}} U_{x\tau_{u_x}i}\, F_{\tau_{u_x}}(x,y)\; \psi_{x_i}(z)\; e^{\imath\,\omega_{ij}\,t} \\ u_y(x,y,z,t) &= \sum_i^{\mathcal{N}} U_{y\tau_{u_y}i}\, F_{\tau_{u_y}}(x,y)\; \psi_{y_i}(z)\; e^{\imath\,\omega_{ij}\,t} \\ u_z(x,y,z,t) &= \sum_i^{\mathcal{N}} U_{z\tau_{u_z}i}\, F_{\tau_{u_z}}(x,y)\; \psi_{z_i}(z)\; e^{\imath\,\omega_{ij}\,t} \end{aligned} \tag{29}$$

and in compact form

$$\mathbf{u} = \mathbf{F}_\tau\, \mathbf{U}_{\tau i}\, \mathbf{\Psi}_i \tag{30}$$

where

$$\mathbf{U}_{\tau i}(t) = \left\{ \begin{array}{c} U_{x\tau_{u_x}i}\; e^{\imath\,\omega_{ij}\,t} \\ U_{y\tau_{u_y}i}\; e^{\imath\,\omega_{ij}\,t} \\ U_{z\tau_{u_z}i}\; e^{\imath\,\omega_{ij}\,t} \end{array} \right\}, \quad \mathbf{\Psi}_i(z) = \left[\begin{array}{ccc} \psi_{x_i}(z) & 0 & 0 \\ 0 & \psi_{y_i}(z) & 0 \\ 0 & 0 & \psi_{z_i(z)} \end{array} \right] \tag{31}$$

The combination of Eqs. (3) and (30) leads to geometrical relations written in terms of Ritz functions

$$\begin{aligned} \boldsymbol{\varepsilon}_{pG} &= \mathbf{D}_p\,(\mathbf{F}_\tau\, \mathbf{\Psi}_i)\; \mathbf{U}_{\tau i} \\ \boldsymbol{\varepsilon}_{nG} &= \mathbf{D}_{np}\,(\mathbf{F}_\tau\, \mathbf{\Psi}_i)\; \mathbf{U}_{\tau i} + \mathbf{D}_{nz}\,(\mathbf{F}_\tau\, \mathbf{\Psi}_i)\; \mathbf{U}_{\tau i} \end{aligned} \tag{32}$$

By substituting the previous expression in Eq. (24) the explicit expressions of the internal work, split in its fourth contributions, and the inertial work are obtained, and assume the following form

$$\begin{aligned} \delta\,(L_{int})_{pp} &= \int_\Omega \int_l \delta\boldsymbol{\varepsilon}_{pG}^T\, \mathbf{C}_{pp}\, \boldsymbol{\varepsilon}_{pG}\, \mathrm{d}\Omega\, \mathrm{d}z \\ &= \delta\mathbf{U}_{\tau i}^T \Big(\int_\Omega \int_l [\mathbf{D}_p\;(\mathbf{F}_\tau\, \mathbf{\Psi}_i)]^T\; \mathbf{C}_{pp}\, \mathbf{D}_p\;(\mathbf{F}_s\, \mathbf{\Psi}_j)\, \mathrm{d}\Omega\, \mathrm{d}z \Big) \mathbf{U}_{sj} \end{aligned}$$

$$
\begin{aligned}
\delta\left(L_{int}\right)_{pn} = & \int_{\Omega}\int_{l}\delta\boldsymbol{\varepsilon}_{pG}^{T}\,\mathbf{C}_{pn}\,\boldsymbol{\varepsilon}_{nG}\,\mathrm{d}\Omega\,\mathrm{d}z \\
= & \,\delta\mathbf{U}_{\tau i}^{T}\Big(\int_{\Omega}\int_{l}\left[\mathbf{D}_{p}\,\left(\mathbf{F}_{\tau}\,\boldsymbol{\Psi}_{i}\right)\right]^{T}\,\mathbf{C}_{pn}\,\mathbf{D}_{np}\,\left(\mathbf{F}_{s}\,\boldsymbol{\Psi}_{j}\right)+ \\
& \qquad\left[\mathbf{D}_{p}\left(\mathbf{F}_{\tau}\,\boldsymbol{\Psi}_{i}\right)\right]^{T}\,\mathbf{C}_{pn}\,\mathbf{D}_{nz}\,\left(\mathbf{F}_{s}\,\boldsymbol{\Psi}_{j}\right)\mathrm{d}\Omega\,\mathrm{d}z\Big)\,\mathbf{U}_{sj}
\end{aligned}
$$

$$
\begin{aligned}
\delta\left(L_{int}\right)_{np} = & \int_{\Omega}\int_{l}\delta\boldsymbol{\varepsilon}_{nG}^{T}\,\mathbf{C}_{np}\,\boldsymbol{\varepsilon}_{pG}\,\mathrm{d}\Omega\,\mathrm{d}z \\
= & \,\delta\mathbf{U}_{\tau i}^{T}\Big(\int_{\Omega}\int_{l}\left[\mathbf{D}_{np}\,\left(\mathbf{F}_{\tau}\,\boldsymbol{\Psi}_{i}\right)\right]^{T}\,\mathbf{C}_{np}\,\mathbf{D}_{p}\,\left(\mathbf{F}_{s}\,\boldsymbol{\Psi}_{j}\right)+ \\
& \qquad\left[\mathbf{D}_{nz}\left(\mathbf{F}_{\tau}\,\boldsymbol{\Psi}_{i}\right)\right]^{T}\,\mathbf{C}_{np}\,\mathbf{D}_{p}\,\left(\mathbf{F}_{s}\,\boldsymbol{\Psi}_{j}\right)\mathrm{d}\Omega\,\mathrm{d}z\Big)\,\mathbf{U}_{sj}
\end{aligned}
\tag{33}
$$

$$
\begin{aligned}
\delta\left(L_{int}\right)_{nn} = & \int_{\Omega}\int_{l}\delta\boldsymbol{\varepsilon}_{nG}^{T}\,\mathbf{C}_{nn}\,\boldsymbol{\varepsilon}_{nG}\,\mathrm{d}\Omega\,\mathrm{d}z \\
= & \,\delta\mathbf{U}_{\tau i}^{T}\Big(\int_{\Omega}\int_{l}\left[\mathbf{D}_{np}\,\left(\mathbf{F}_{\tau}\,\boldsymbol{\Psi}_{i}\right)\right]^{T}\,\mathbf{C}_{nn}\,\mathbf{D}_{np}\,\left(\mathbf{F}_{s}\,\boldsymbol{\Psi}_{j}\right)+ \\
& \qquad\left[\mathbf{D}_{np}\left(\mathbf{F}_{\tau}\,\boldsymbol{\Psi}_{i}\right)\right]^{T}\,\mathbf{C}_{nn}\,\mathbf{D}_{nz}\,\left(\mathbf{F}_{s}\,\boldsymbol{\Psi}_{j}\right)+ \\
& \qquad\left[\mathbf{D}_{nz}\left(\mathbf{F}_{\tau}\,\boldsymbol{\Psi}_{i}\right)\right]^{T}\,\mathbf{C}_{nn}\,\mathbf{D}_{np}\,\left(\mathbf{F}_{s}\,\boldsymbol{\Psi}_{j}\right)+ \\
& \qquad\left[\mathbf{D}_{nz}\left(\mathbf{F}_{\tau}\,\boldsymbol{\Psi}_{i}\right)\right]^{T}\,\mathbf{C}_{nn}\,\mathbf{D}_{nz}\,\left(\mathbf{F}_{s}\,\boldsymbol{\Psi}_{j}\right)\mathrm{d}\Omega\,\mathrm{d}z\Big)\,\mathbf{U}_{sj}
\end{aligned}
$$

$$
\delta L_{F_{in}} = \delta\mathbf{U}_{\tau i}^{T}\Big[\int_{\Omega}\int_{l}\rho\left(\mathbf{F}_{\tau}\boldsymbol{\Psi}_{i}\right)^{T}\left(\mathbf{F}_{s}\boldsymbol{\Psi}_{j}\right)\mathrm{d}\Omega\,\mathrm{d}z\Big]\ddot{\mathbf{U}}_{sj}
$$

The internal and inertial virtual works can be written as

$$
\begin{aligned}
\delta L_{int} &= \delta\left(L_{int}\right)_{pp}+\delta\left(L_{int}\right)_{pn}+\delta\left(L_{int}\right)_{np}+\delta\left(L_{int}\right)_{nn} \\
&= \delta\mathbf{U}_{\tau i}^{T}\Big(\mathbf{K}_{pp}^{\tau sij}+\mathbf{K}_{pn}^{\tau sij}+\mathbf{K}_{np}^{\tau sij}+\mathbf{K}_{nn}^{\tau sij}\Big)\,\mathbf{U}_{sj} \\
&= \delta\mathbf{U}_{\tau i}^{T}\,\mathbf{K}^{\tau sij}\,\mathbf{U}_{sj}
\end{aligned}
\tag{34}
$$

$$
\delta L_{F_{in}} = \delta\mathbf{U}_{\tau i}^{T}\,\mathbf{M}^{\tau sij}\,\ddot{\mathbf{U}}_{sj}
$$

Then by comparing Eqs.(33) and (34), the Ritz fundamental primary stiffness and mass nuclei are obtained

$$
\mathbf{K}_{pp}^{\tau sij} = \Big(\left[\mathbf{D}_{p}\left(\mathbf{F}_{\tau}\,\boldsymbol{\Psi}_{i}\right)\right]^{T}\,\mathbf{C}_{pp}\mathbf{D}_{p}\left(\mathbf{F}_{s}\,\boldsymbol{\Psi}_{j}\right)\Big)
$$

$$\mathbf{K}_{pn}^{\tau sij} = \Big(\left[\mathbf{D}_p \left(\mathbf{F}_\tau \, \mathbf{\Psi}_i\right)\right]^T \, \mathbf{C}_{pn} \mathbf{D}_{np} \left(\mathbf{F}_s \, \mathbf{\Psi}_j\right) + \left[\mathbf{D}_p \left(\mathbf{F}_\tau \, \mathbf{\Psi}_i\right)\right]^T \, \mathbf{C}_{pn} \mathbf{D}_{nz} \left(\mathbf{F}_s \, \mathbf{\Psi}_j\right) \Big)$$

$$\mathbf{K}_{np}^{\tau sij} = \Big(\left[\mathbf{D}_{np} \left(\mathbf{F}_\tau \, \mathbf{\Psi}_i\right)\right]^T \, \mathbf{C}_{np} \mathbf{D}_p \left(\mathbf{F}_s \, \mathbf{\Psi}_j\right) + \left[\mathbf{D}_{nz} \left(\mathbf{F}_\tau \, \mathbf{\Psi}_i\right)\right]^T \, \mathbf{C}_{np} \mathbf{D}_p \left(\mathbf{F}_s \, \mathbf{\Psi}_j\right) \Big) \tag{35}$$

$$\begin{aligned} \mathbf{K}_{nn}^{\tau sij} = \Big(& \left[\mathbf{D}_{np} \left(\mathbf{F}_\tau \, \mathbf{\Psi}_i\right)\right]^T \, \mathbf{C}_{nn} \mathbf{D}_{np} \left(\mathbf{F}_s \, \mathbf{\Psi}_j\right) + \left[\mathbf{D}_{np} \left(\mathbf{F}_\tau \, \mathbf{\Psi}_i\right)\right]^T \, \mathbf{C}_{nn} \mathbf{D}_{nz} \left(\mathbf{F}_s \, \mathbf{\Psi}_j\right) \\ & + \left[\mathbf{D}_{nz} \left(\mathbf{F}_\tau \, \mathbf{\Psi}_i\right)\right]^T \, \mathbf{C}_{nn} \mathbf{D}_{np} \left(\mathbf{F}_s \, \mathbf{\Psi}_j\right) + \left[\mathbf{D}_{nz} \left(\mathbf{F}_\tau \, \mathbf{\Psi}_i\right)\right]^T \, \mathbf{C}_{nn} \mathbf{D}_{nz} \left(\mathbf{F}_s \, \mathbf{\Psi}_j\right) \Big) \end{aligned}$$

Summing the different contributions the final form of the primary stiffness nucleus is

$$\mathbf{K}^{\tau sij} = \mathbf{K}_{pp}^{\tau sij} + \mathbf{K}_{pn}^{\tau sij} + \mathbf{K}_{np}^{\tau sij} + \mathbf{K}_{nn}^{\tau sij} \tag{36}$$

and the its explicit form along with the one of the primary mass nucleus are following given

$$\begin{aligned} \mathbf{K}^{\tau sij} = \int_\Omega \int_l \Big(& \left[\mathbf{D}_p \left(\mathbf{F}_\tau \, \mathbf{\Psi}_i\right)\right]^T \left[\mathbf{C}_{pp} \mathbf{D}_p \left(\mathbf{F}_s \, \mathbf{\Psi}_j\right) + \mathbf{C}_{pn} \mathbf{D}_{np} \left(\mathbf{F}_s \, \mathbf{\Psi}_j\right) + \mathbf{C}_{pn} \mathbf{D}_{nz} \left(\mathbf{F}_s \, \mathbf{\Psi}_j\right)\right] \\ & + \left[\mathbf{D}_{np} \left(\mathbf{F}_\tau \, \mathbf{\Psi}_i\right)\right]^T \left[\mathbf{C}_{np} \mathbf{D}_p \left(\mathbf{F}_s \, \mathbf{\Psi}_j\right) + \mathbf{C}_{nn} \mathbf{D}_{np} \left(\mathbf{F}_s \, \mathbf{\Psi}_j\right) + \mathbf{C}_{nn} \mathbf{D}_{nz} \left(\mathbf{F}_s \, \mathbf{\Psi}_j\right)\right] \\ & + \left[\mathbf{D}_{nz} \left(\mathbf{F}_\tau \, \mathbf{\Psi}_i\right)\right]^T \left[\mathbf{C}_{np} \mathbf{D}_p \left(\mathbf{F}_s \, \mathbf{\Psi}_j\right) + \mathbf{C}_{nn} \mathbf{D}_{np} \left(\mathbf{F}_s \, \mathbf{\Psi}_j\right) + \mathbf{C}_{nn} \mathbf{D}_{nz} \left(\mathbf{F}_s \, \mathbf{\Psi}_j\right)\right] \Big) \, \mathrm{d}\Omega \, \mathrm{d}z \end{aligned} \tag{37}$$

$$\mathbf{M}^{\tau sij} = \int_\Omega \int_l \Big(\rho \left[\left(\mathbf{F}_\tau \mathbf{\Psi}_i\right)^T \left(\mathbf{F}_s \mathbf{\Psi}_j\right) \right] \Big) \, \mathrm{d}\Omega \, \mathrm{d}z$$

After performing the matrix calculus in Eq. (37) the nine secondary stiffness nuclei are obtained

$$\begin{aligned} K_{u_x u_x}^{\tau_{u_x} s_{u_x}} = & C_{11} \int_\Omega F_{\tau_{u_{x,x}}} \, F_{s_{u_{x,x}}} \mathrm{d}\Omega \int_l \psi_{x_i} \, \psi_{x_j} \mathrm{d}z + C_{16} \int_\Omega F_{\tau_{u_{x,y}}} \, F_{s_{u_{x,x}}} \mathrm{d}\Omega \int_l \psi_{x_i} \, \psi_{x_j} \mathrm{d}z \\ & + C_{16} \int_\Omega F_{\tau_{u_{x,x}}} \, F_{s_{u_{x,y}}} \mathrm{d}\Omega \int_l \psi_{x_i} \, \psi_{x_j} \mathrm{d}z + C_{66} \int_\Omega F_{\tau_{u_{x,y}}} \, F_{s_{u_{x,y}}} \mathrm{d}\Omega \int_l \psi_{x_i} \, \psi_{x_j} \mathrm{d}z \\ & + C_{55} \int_\Omega F_{\tau_{u_x}} \, F_{s_{u_x}} \mathrm{d}\Omega \int_l \psi_{x_{i,z}} \, \psi_{x_{j,z}} \mathrm{d}z \end{aligned}$$

$$\begin{aligned} K_{u_x u_y}^{\tau_{u_x} s_{u_y}} = & C_{12} \int_\Omega F_{\tau_{u_{x,x}}} \, F_{s_{u_{y,y}}} \mathrm{d}\Omega \int_l \psi_{x_i} \, \psi_{y_j} \mathrm{d}z + C_{26} \int_\Omega F_{\tau_{u_{x,y}}} \, F_{s_{u_{y,y}}} \mathrm{d}\Omega \int_l \psi_{x_i} \, \psi_{y_j} \mathrm{d}z \\ & + C_{16} \int_\Omega F_{\tau_{u_{x,x}}} \, F_{s_{u_{y,x}}} \mathrm{d}\Omega \int_l \psi_{x_i} \, \psi_{y_j} \mathrm{d}z + C_{66} \int_\Omega F_{\tau_{u_{x,y}}} \, F_{s_{u_{y,x}}} \mathrm{d}\Omega \int_l \psi_{x_i} \, \psi_{y_j} \mathrm{d}z \\ & + C_{45} \int_\Omega F_{\tau_{u_x}} \, F_{s_{u_y}} \mathrm{d}\Omega \int_l \psi_{x_{i,z}} \, \psi_{y_{j,z}} \mathrm{d}z \end{aligned}$$

$$
\begin{aligned}
K_{u_x u_z}^{\tau_{u_x} s_{u_z}} &= C_{13} \int_\Omega F_{\tau_{u_{x,x}}} F_{s_{u_z}} \mathrm{d}\Omega \int_l \psi_{x_i} \psi_{z_{j,z}} \mathrm{d}z + C_{36} \int_\Omega F_{\tau_{u_{x,y}}} F_{s_{u_z}} \mathrm{d}\Omega \int_l \psi_{x_i} \psi_{z_{j,z}} \mathrm{d}z \\
&+ C_{55} \int_\Omega F_{\tau_{u_x}} F_{s_{u_{z,x}}} \mathrm{d}\Omega \int_l \psi_{x_{i,z}} \psi_{z_j} \mathrm{d}z + C_{45} \int_\Omega F_{\tau_{u_x}} F_{s_{u_{z,y}}} \mathrm{d}\Omega \int_l \psi_{x_{i,z}} \psi_{z_j} \mathrm{d}z
\end{aligned}
$$

$$
\begin{aligned}
K_{u_y u_x}^{\tau_{u_y} s_{u_x}} &= C_{12} \int_\Omega F_{\tau_{u_{y,y}}} F_{s_{u_{x,x}}} \mathrm{d}\Omega \int_l \psi_{y_i} \psi_{x_j} \mathrm{d}z + C_{16} \int_\Omega F_{\tau_{u_{y,x}}} F_{s_{u_{x,x}}} \mathrm{d}\Omega \int_l \psi_{y_i} \psi_{x_j} \mathrm{d}z \\
&+ C_{26} \int_\Omega F_{\tau_{u_{y,y}}} F_{s_{u_{x,y}}} \mathrm{d}\Omega \int_l \psi_{y_i} \psi_{x_j} \mathrm{d}z + C_{66} \int_\Omega F_{\tau_{u_{y,x}}} F_{s_{u_{x,y}}} \mathrm{d}\Omega \int_l \psi_{y_i} \psi_{x_j} \mathrm{d}z \\
&+ C_{45} \int_\Omega F_{\tau_{u_y}} F_{s_{u_x}} \mathrm{d}\Omega \int_l \psi_{y_{i,z}} \psi_{x_{j,z}} \mathrm{d}z
\end{aligned}
$$

$$
\begin{aligned}
K_{u_y u_y}^{\tau_{u_y} s_{u_y}} &= C_{22} \int_\Omega F_{\tau_{u_{y,y}}} F_{s_{u_{y,y}}} \mathrm{d}\Omega \int_l \psi_{y_i} \psi_{y_j} \mathrm{d}z + C_{26} \int_\Omega F_{\tau_{u_{y,x}}} F_{s_{u_{y,y}}} \mathrm{d}\Omega \int_l \psi_{y_i} \psi_{y_j} \mathrm{d}z \\
&+ C_{26} \int_\Omega F_{\tau_{u_{y,y}}} F_{s_{u_{y,x}}} \mathrm{d}\Omega \int_l \psi_{y_i} \psi_{y_j} \mathrm{d}z + C_{66} \int_\Omega F_{\tau_{u_{y,x}}} F_{s_{u_{y,x}}} \mathrm{d}\Omega \int_l \psi_{y_i} \psi_{y_j} \mathrm{d}z \\
&+ C_{44} \int_\Omega F_{\tau_{u_y}} F_{s_{u_y}} \mathrm{d}\Omega \int_l \psi_{y_{i,z}} \psi_{y_{j,z}} \mathrm{d}z
\end{aligned}
$$

$$
\begin{aligned}
K_{u_y u_z}^{\tau_{u_y} s_{u_z}} &= C_{23} \int_\Omega F_{\tau_{u_{y,y}}} F_{s_{u_z}} \mathrm{d}\Omega \int_l \psi_{y_i} \psi_{z_{j,z}} \mathrm{d}z + C_{36} \int_\Omega F_{\tau_{u_{y,x}}} F_{s_{u_z}} \mathrm{d}\Omega \int_l \psi_{y_i} \psi_{z_{j,z}} \mathrm{d}z \\
&+ C_{45} \int_\Omega F_{\tau_{u_y}} F_{s_{u_{z,x}}} \mathrm{d}\Omega \int_l \psi_{y_{i,z}} \psi_{z_j} \mathrm{d}z + C_{44} \int_\Omega F_{\tau_{u_y}} F_{s_{u_{z,y}}} \mathrm{d}\Omega \int_l \psi_{y_{i,z}} \psi_{z_j} \mathrm{d}z
\end{aligned} \tag{38}
$$

$$
\begin{aligned}
K_{u_z u_x}^{\tau_{u_z} s_{u_x}} &= C_{55} \int_\Omega F_{\tau_{u_{z,x}}} F_{s_{u_x}} \mathrm{d}\Omega \int_l \psi_{z_i} \psi_{x_{j,z}} \mathrm{d}z + C_{45} \int_\Omega F_{\tau_{u_{z,y}}} F_{s_{u_x}} \mathrm{d}\Omega \int_l \psi_{z_i} \psi_{x_{j,z}} \mathrm{d}z \\
&+ C_{13} \int_\Omega F_{\tau_{u_z}} F_{s_{u_{x,x}}} \mathrm{d}\Omega \int_l \psi_{z_{i,z}} \psi_{x_j} \mathrm{d}z + C_{36} \int_\Omega F_{\tau_{u_z}} F_{s_{u_{x,y}}} \mathrm{d}\Omega \int_l \psi_{z_{i,z}} \psi_{x_j} \mathrm{d}z
\end{aligned}
$$

$$
\begin{aligned}
K_{u_z u_y}^{\tau_{u_z} s_{u_y}} &= C_{45} \int_\Omega F_{\tau_{u_{z,x}}} F_{s_{u_y}} \mathrm{d}\Omega \int_l \psi_{z_i} \psi_{y_{j,z}} \mathrm{d}z + C_{44} \int_\Omega F_{\tau_{u_{z,y}}} F_{s_{u_y}} \mathrm{d}\Omega \int_l \psi_{z_i} \psi_{y_{j,z}} \mathrm{d}z \\
&+ C_{23} \int_\Omega F_{\tau_{u_z}} F_{s_{u_{y,y}}} \mathrm{d}\Omega \int_l \psi_{z_{i,z}} \psi_{y_j} \mathrm{d}z + C_{36} \int_\Omega F_{\tau_{u_z}} F_{s_{u_{y,x}}} \mathrm{d}\Omega \int_l \psi_{z_{i,z}} \psi_{y_j} \mathrm{d}z
\end{aligned}
$$

$$
\begin{aligned}
K_{u_z u_z}^{\tau_{u_z} s_{u_z}} &= C_{55} \int_\Omega F_{\tau_{u_{z,x}}} F_{s_{u_{z,x}}} \mathrm{d}\Omega \int_l \psi_{z_i} \psi_{z_j} \mathrm{d}z + C_{45} \int_\Omega F_{\tau_{u_{z,y}}} F_{s_{u_{z,x}}} \mathrm{d}\Omega \int_l \psi_{z_i} \psi_{z_j} \mathrm{d}z \\
&+ C_{45} \int_\Omega F_{\tau_{u_{z,x}}} F_{s_{u_{z,y}}} \mathrm{d}\Omega \int_l \psi_{z_i} \psi_{z_j} \mathrm{d}z + C_{44} \int_\Omega F_{\tau_{u_{z,y}}} F_{s_{u_{z,y}}} \mathrm{d}\Omega \int_l \psi_{z_i} \psi_{z_j} \mathrm{d}z \\
&+ C_{33} \int_\Omega F_{\tau_{u_z}} F_{s_{u_z}} \mathrm{d}\Omega \int_l \psi_{z_{i,z}} \psi_{z_{j,z}} \mathrm{d}z
\end{aligned}
$$

It should be noted that in the case of the FG beams the elastic coefficients must be integrated along with the cross-section functions. In order to write the nine primary nucleus components in a more concise way, a compact notation, for both line and surface integrals, is introduced. In particular, as regard the surface integrals the following expression is used

$$J^{\tau,\zeta s,\eta} = \int_{\Omega} F_{\tau,\zeta} F_{s,\eta} \mathrm{d}\Omega \quad \tau = \tau_{u_x}, \tau_{u_y}, \tau_{u_z}; \;\; s = s_{u_x}, s_{u_y}, s_{u_z}; \tag{39}$$

where $,\zeta$ and $,\eta$ represent differentiation with respect to that variable. The line integrals are instead contracted as follows

$$I_{pq}^{\chi\xi} = \int_0^l \frac{\mathrm{d}^{\chi}\psi_{p_i}(z)}{\mathrm{d}z^{\chi}} \frac{\mathrm{d}^{\xi}\psi_{q_j}(z)}{\mathrm{d}z^{\xi}} \mathrm{d}z \quad i = 1, \cdots, \mathcal{M}; \;\; j = 1, \cdots, \mathcal{N}; \tag{40}$$

where $p, q = u_x, u_y, u_z$; χ and ξ indicate differentiation orders; and $\mathcal{M}$ and $\mathcal{N}$ represent the Ritz expansion orders. Substituting Eqs. (39) and (40) in Eq. (38) the compact form of the primary stiffness nucleus components is obtained as follows

$$\begin{aligned}
K_{u_x u_x}^{\tau_{u_x} s_{u_x}} &= C_{11} J^{\tau_{u_x,x}\, s_{u_x,x}} I_{u_x u_x}^{00} + C_{16} J^{\tau_{u_x,y}\, s_{u_x,x}} I_{u_x u_x}^{00} + C_{16} J^{\tau_{u_x,x}\, s_{u_x,y}} I_{u_x u_x}^{00} \\
&+ C_{66} J^{\tau_{u_x,y}\, s_{u_x,y}} I_{u_x u_x}^{00} + C_{55} J^{\tau_{u_x} s_{u_x}} I_{u_x u_x}^{11} \\
\\
K_{u_x u_y}^{\tau_{u_x} s_{u_y}} &= C_{12} J^{\tau_{u_x,x}\, s_{u_y,y}} I_{u_x u_y}^{00} + C_{26} J^{\tau_{u_x,y}\, s_{u_y,y}} I_{u_x u_y}^{00} + C_{16} J^{\tau_{u_x,x}\, s_{u_y,x}} I_{u_x u_y}^{00} \\
&+ C_{66} J^{\tau_{u_x,y}\, s_{u_y,x}} I_{u_x u_y}^{00} + C_{45} J^{\tau_{u_x} s_{u_y}} I_{u_x u_y}^{11} \\
\\
K_{u_x u_z}^{\tau_{u_x} s_{u_z}} &= C_{13} J^{\tau_{u_x,x}\, s_{u_z}} I_{u_x u_z}^{01} + C_{36} J^{\tau_{u_x,y}\, s_{u_z}} I_{u_x u_z}^{01} + C_{55} J^{\tau_{u_x} s_{u_z,x}} I_{u_x u_z}^{10} \\
&+ C_{45} J^{\tau_{u_x} s_{u_z,y}} I_{u_x u_z}^{10} \\
\\
K_{u_y u_x}^{\tau_{u_y} s_{u_x}} &= C_{12} J^{\tau_{u_y,y}\, s_{u_x,x}} I_{u_y u_x}^{00} + C_{16} J^{\tau_{u_y,x}\, s_{u_x,x}} I_{u_y u_x}^{00} + C_{26} J^{\tau_{u_y,y}\, s_{u_x,y}} I_{u_y u_x}^{00} \\
&+ C_{66} J^{\tau_{u_y,x}\, s_{u_x,y}} I_{u_y u_x}^{00} + C_{45} J^{\tau_{u_y} s_{u_x}} I_{u_y u_x}^{11} \\
\\
K_{u_y u_y}^{\tau_{u_y} s_{u_y}} &= C_{22} J^{\tau_{u_y,y}\, s_{u_y,y}} I_{u_y u_y}^{00} + C_{26} J^{\tau_{u_y,x}\, s_{u_y,y}} I_{u_y u_y}^{00} + C_{26} J^{\tau_{u_y,y}\, s_{u_y,x}} I_{u_y u_y}^{00} \\
&+ C_{66} J^{\tau_{u_y,x}\, s_{u_y,x}} I_{u_y u_y}^{00} + C_{44} J^{\tau_{u_y} s_{u_y}} I_{u_y u_y}^{11} \\
\\
K_{u_y u_z}^{\tau_{u_y} s_{u_z}} &= C_{23} J^{\tau_{u_y,y}\, s_{u_z}} I_{u_y u_z}^{01} + C_{36} J^{\tau_{u_y,x}\, s_{u_z}} I_{u_y u_z}^{01} + C_{45} J^{\tau_{u_y} s_{u_z,x}} I_{u_y u_z}^{10} \\
&+ C_{44} J^{\tau_{u_y} s_{u_z,y}} I_{u_y u_z}^{10}
\end{aligned} \tag{41}$$

$$K_{u_z u_x}^{\tau_{u_z} s_{u_x}} = C_{55} J^{\tau_{u_z,x}\, s_{u_x}} I_{u_z u_x}^{01} + C_{45} J^{\tau_{u_z,y}\, s_{u_x}} I_{u_z u_x}^{01} + C_{13} J^{\tau_{u_z}\, s_{u_x,x}} I_{u_z u_x}^{10} + C_{36} J^{\tau_{u_z}\, s_{u_x,y}} I_{u_z u_x}^{10}$$

$$K_{u_z u_y}^{\tau_{u_z} s_{u_y}} = C_{45} J^{\tau_{u_z,x}\, s_{u_x}} I_{u_z u_y}^{01} + C_{44} J^{\tau_{u_z,y}\, s_{u_y}} I_{u_z u_y}^{01} + C_{23} J^{\tau_{u_z}\, s_{u_y,y}} I_{u_z u_y}^{10} + C_{36} J^{\tau_{u_z}\, s_{u_y,x}} I_{u_z u_y}^{10}$$

$$K_{u_z u_z}^{\tau_{u_z} s_{u_z}} = C_{55} J^{\tau_{u_z,x}\, s_{u_z,x}} I_{u_z u_z}^{00} + C_{45} J^{\tau_{u_z,y}\, s_{u_z,x}} I_{u_z u_z}^{00} + C_{45} J^{\tau_{u_z,x}\, s_{u_z,y}} I_{u_z u_z}^{00} + C_{44} J^{\tau_{u_z,y}\, s_{u_z,y}} I_{u_z u_z}^{00} + C_{33} J^{\tau_{u_z}\, s_{u_z}} I_{u_z u_z}^{11}$$

Following a similar approach, the nine primary mass nucleus components, in their unabridged form, are given as follows

$$\begin{array}{lll} M_{u_x u_x}^{\tau_{u_x} s_{u_x}} = \rho\, J^{\tau_{u_x}\, s_{u_x}} I_{u_x u_x}^{00} & M_{u_x u_y}^{\tau_{u_x} s_{u_y}} = 0 & M_{u_x u_z}^{\tau_{u_x} s_{u_z}} = 0 \\ M_{u_y u_x}^{\tau_{u_y} s_{u_x}} = 0 & M_{u_y u_y}^{\tau_{u_y} s_{u_y}} = \rho\, J^{\tau_{u_y}\, s_{u_y}} I_{u_y u_y}^{00} & M_{u_y u_z}^{\tau_{u_y} s_{u_z}} = 0 \\ M_{u_z u_x}^{\tau_{u_z} s_{u_x}} = 0 & M_{u_z u_y}^{\tau_{u_z} s_{u_y}} = 0 & M_{u_z u_z}^{\tau_{u_z} s_{u_z}} = \rho\, J^{\tau_{u_z}\, s_{u_z}} I_{u_z u_z}^{00} \end{array} \tag{42}$$

4.2. Algebraic Ritz Functions and Gram-Schmidt process

The Ritz functions used in the present article are a set of algebraic functions which satisfy the geometric boundary conditions. In particular, they assume the following form

$$\begin{aligned} \psi_{x_i}(z) &= z^{p_x} (l-z)^{q_x} z^{i-1} \quad i = 1, 2, 3, \cdots, \mathcal{N} \\ \psi_{y_i}(z) &= z^{p_y} (l-z)^{q_y} z^{i-1} \quad i = 1, 2, 3, \cdots, \mathcal{N} \\ \psi_{z_i}(z) &= z^{p_z} (l-z)^{q_z} z^{i-1} \quad i = 1, 2, 3, \cdots, \mathcal{N} \end{aligned} \tag{43}$$

Where $\mathcal{N}$ is the expansion order in the Ritz approximation, l is the length of the beam, p_k and q_k, with $k = x$, y, z, assume the values $0, 1, 2$ for free (F), simply supported (SS) and clamped (C) boundary conditions, respectively.

In order to enhance significantly the computational stability, the Ritz functions have been orthogonalized in the domain ($z \in [0, l]$) via the Gram-Smith process [68]. The first member of the orthogonal polynomial set $\psi_{x_1}(z)$ is chosen as the simplest polynomial of the least order that satisfies both the geometrical and the natural boundary conditions of the beam. The other members of the orthogonal set in the interval $0 \leq z \leq l$ are generated by using

the Gram-Schmidt process as follows

$$\begin{aligned}
&\psi_{x_2}(z) = (z - B_2)\,\psi_{x_1}(z)\,,\\
&\psi_{x_3}(z) = (z - B_3)\,\psi_{x_2}(z) - C_3\,\psi_{x_1}(z)\,,\\
&\vdots\\
&\psi_{x_i}(z) = (z - B_i)\,\psi_{x_{i-1}}(z) - C_i\,\psi_{x_{i-2}}(z)\\
&\vdots\\
&\psi_{x_{\mathcal{N}}}(z) = (z - B_{\mathcal{N}})\,\psi_{x_{\mathcal{N}-1}}(z) - C_{\mathcal{N}}\,\psi_{x_{\mathcal{N}-2}}(z)
\end{aligned} \tag{44}$$

where

$$B_i = \frac{\left[\int_0^l w(z)\; z\,\psi^2_{x_{i-1}}(z)\;\mathrm{d}z\right]}{\left[\int_0^l w(z)\;\psi^2_{x_{i-1}}(z)\;\mathrm{d}z\right]} \tag{45}$$

and

$$C_i = \frac{\left[\int_0^l w(z)\; z\,\psi_{x_{i-1}}(z)\;\psi_{x_{i-2}}(z)\;\mathrm{d}z\right]}{\left[\int_0^l w(z)\;\psi^2_{x_{i-2}}(z)\;\mathrm{d}z\right]} \tag{46}$$

The polynomials ψ_{x_i} satisfy the orthogonality condition

$$\int_0^l w(z)\;\psi_{x_i}(z)\;\psi_{x_j}(z)\,\mathrm{d}z = \delta_{ij} \tag{47}$$

where δ_{ij} is kroneker's delta and $w(z)$ is the weight function. In the particular case of uniform beams $w(z) = 1$. The same process has been applied for the orthogonalization of the Ritz functions $\psi_{y_i}(z)$ and $\psi_{z_i}(z)$ with $i = 1, 2, 3, \cdots, \mathcal{N}$.

5. Numerical results and discussion

In the present section the developed refined and advanced quasi-3D beam models are validated and assessed by using both results obtained via commercial FEM software (ABAQUS and ANSYS) and results available in the literature. In particular, two case-studies, concerning with the free vibration analysis of metallic and FG beams, are proposed.

1. **case study**

   The analysis is focused on the computation of eigenfrequencies of a metallic beam with various boundary conditions (see Table 2) made up of aluminium alloy, with Young's modulus $E = 69\,GPa$, Poisson's ratio $\nu = 0.33$ and density $\rho = 2700\,Kg/m^3$. The geometrical characteristics are $h = 0.1\,m$, $b = 1\,m$ and $l = 10\,m$.

2. **case study**

   The analysis is devoted to the calculation of eigenfrequencies of FG beams with various boundary conditions. The FG beam is made up of stainless steal (SUS304) as metal and alumina (Al_2O_3) as ceramic. The material properties of the stainless steal are $E_m = 210\,GPa$, $\nu_m = 0.31$, and $\rho_m = 7800\,Kg/m^3$, and those of the alumina are $E_m = 390\,GPa$, $\nu_c = 0.25$, and $\rho_c = 3960\,Kg/m^3$ [37].

The results are given using the acronym $TE_{N_{u_x}N_{u_y}N_{u_z}}$ where TE states that Taylor's series expansion is used to describe the displacement field over the beam cross-section and N_{u_x}, N_{u_y} and N_{u_z} are the three independent expansion orders used in the beam model.
In the proposed analysis, the discrepancy between the results obtained by using the developed beam models (f_p) and those computed using FEM software and/or selected from the literature (f_o), is evaluated as follows

$$\text{Rel. Diff}\,(\%) = \frac{\|f_p - f_o\|}{\|f_o\|} \times 100 \tag{48}$$

5.1. Convergence analysis

A comprehensive convergence analysis of the algebraic Ritz functions used in the analysis has been carried out for a cantilever rectangular beam (CF) with material and geometrical characteristics equal to those provided in the *case study 1*. The expansion indexes i and j in the Ritz functions are progressively increased from 2 to 18, namely till convergence is reached, and the results of the analysis have been proposed in Table 3. Nine different beam theories accounting for distinct expansion orders have been tested for both lower (f_1) and higher (f_7) modes. The analysis showed some interesting results. The rate of convergence is higher for higher modes and is also slightly affected by the selected beam theory. Higher-order beam models are mandatory for accurately describe mode shapes which involve torsion, distortion and warping of the beam cross-section. An example is the torsional mode f_7, indeed, in this case the addition of degrees of freedom (DOFs) over the beam cross-section leads to a remarkable enhancement in the results accuracy while any refinement in the Ritz approximation does not affect significantly the results accuracy. In sharp contrast, bending modes are instead accurately described by lower-order beam models and further significant improvements can only be achieved by increasing the number of DOFs in the Ritz expansion. These conclusions can be drawn by comparing the beam model TE_{333} and TE_{999} with the 3D FEM solutions. More specifically, in the computation of the fundamental frequency, related

to a bending mode in the $xz-$plane, the discrepancies of the beam theories with respect to the 3D FEM is 0.56% and 0.43%, respectively. Namely, they lead to the same level of accuracy then the use of the more expensive TE_{999} beam theory can be avoided. On the contrary, the use of the later becomes instead mandatory when the torsional mode (f_7) is computed, indeed the difference between the two discrepancies become remarkable, that is, 1.98% and 0.26%, respectively.

5.2. Effectiveness of higher-order beam models

An example of study of the effectiveness of the higher-order terms in the beam models is provided in Table 4. The beam under investigation has the same geometrical and material characteristics of that studied in the convergence analysis. In this case the first ten natural frequencies have been computed using different beam models and the results have been compared with those evaluated by using ABAQUS and ANSYS. The use of distinct expansion orders permits to evaluate the effectiveness of certain DOFs. In particular, the refinement of the beam cross-section displacement components u_x and u_y, in a separate way, (see the beam theory TE_{422} and TE_{242}) does not produce any improvement in the results accuracy, on the contrary the latter is significantly affect by refining the axial displacement u_z (see the TE_{223} and TE_{224} beam theory). By means of this approach several DOFs can be saved reducing significantly the computational cost. In this respect, it is interesting to observe in Table 4 that, for $i = j = 18$ in the Ritz expansion, the TE_{223} beam theory (396 DOFs) leads to the same level of accuracy of the TE_{333} beam theory (540 DOFs). A further article exclusively focused on this aspect will be proposed in the future. However, in the case of static analysis, results based on the Axiomatic/Asymptotic Method (AAM) using a different approach have been given in Ref. [12].

5.3. Eigenfrequencies and mode shapes of metallic beams

In the *case study 1* the first ten natural frequencies of rectangular metallic beams are computed for different boundary conditions and the related mode shapes are showed in Fig. 4. In particular, from Table 5 to 9 the CC, CS, SS, SF and FF boundary conditions are investigated, respectively. The developed beam theories are assessed towards the 3D FEM results obtained by using ABAQUS. More specifically, the brick element C3DR20 with 20 nodes has been used and a mesh of $5 \times 5 \times 50$ has been applied, with a total number of 37593 DOFs. The most refined beam model involved in the present analysis is the TE_{999} and

associated with $i = j = 18$ in the Ritz expansion, involves a total of 2970 DOFs. Despite the huge discrepancy in the number of the DOFs used in the analysis the proposed sets of results are in an excellent agreement. In all of the cases addressed the average difference percentage never exceed the 1% in the lower-order beam theory TE_{333} and becomes almost zero in the higher-order theory TE_{999}.

5.4. Eigenfrequencies and mode shapes of FG beams

As mentioned before in the *case study 2* the modal characteristics of FG beams are investigated. If not differently stated the results are proposed in terms of dimensionless circular frequency parameters $\hat{\omega} = \omega \frac{l^2}{a}\sqrt{\frac{\rho_m}{E_m}}$. A first validation has been proposed in Table 10. The results, in terms of the first four dimensionless circular frequency parameters, obtained by using the present Ritz formulation for the case of SS boundary condition and volume fraction index $p = 1$, are compared with the analytical solution given in Ref. [37]. In particular, the results make reference to a FG beam with a square cross section. In the analytical solution the half-wave number has been set to be one. Of the first four dimensionless circular frequency parameters proposed, the first two are related to bending modes, in the yz and xz planes, respectively; the third mode is a torsional mode and the fourth is an axial mode. The results showed a perfect match for all of the slenderness ratio values ($l/h = 5$, 10, 100) taken into account.

In the Table 11 the first six dimensionless circular frequency parameters of short FG square beams ($l/h = 5$) are computed by using the present TE_{999} beam model with $i = j = 18$ (2970 DOFs) and ABAQUS. In the latter case the brick element C3DR20 with 20 nodes has been used and a mesh of $10 \times 10 \times 50$ has been applied (70323 DOFs). The results compared for both CF and FF boundary conditions are found to be in an excellent agreement. The average difference percentages are 1.06% and 1.62%, respectively. It should be noted that the FEM accuracy is significantly affected by the FGM implementation in the FEM software. The mode shapes related to the first six dimensionless circular frequency parameters for CF and FF boundary conditions are depicted in Figs. 5 and 6, respectively.

The first five dimensionless circular frequency parameters for both short ($l/h = 5$) and slender ($l/h = 20$) beams, and for CF, CC and CS boundary conditions are given in Tables 12, 13 and 14, respectively. The results obtained by using the present TE_{333} beam theory have been compared with those proposed in Ref. [15] and computed by using the TBT combined with the dynamic stiffness method (DSM). The two sets of results are in an excellent agreement,

for all of the different values of the volume fraction index p taken into account and indeed in all of the studied cases the average relative difference percentage is significantly below the 1% and the maximum relative difference percentage does not exceed the 1.5%. It can be observed in the same tables that dimensionless circular frequency parameters decrease when increasing the volume fraction index p and increase when increasing the slenderness ratio l/h.

6. Conclusions

The free vibration characteristics of metallic and FG short and slender beams with arbitrary boundary conditions have been investigated. The analysis has been carried out by using advanced and refined quasi-3D beam models developed by using a Taylor series expansion. The governing equations have been derived in their week-from by virtue of the Principle of the Virtual Displacements (PVD) and the Ritz method has been used as solution technique. Algebraic Ritz functions, orthogonalised by using the Gram-Schmidt process, have been employed in the approximation. The effect of significant parameters such length-to-thickness ratio, volume fraction index, materials and boundary conditions, have been commented.

The results showed that the rate of convergence is higher for higher modes and is also slightly affected by the selected beam theory. Higher-order beam models are mandatory for accurately describe mode shapes which involve torsion, distortion and warping of the beam cross-section. Moreover, in the latter case any refinement in the Ritz approximation does not affect significantly the results accuracy while the addition of DOFs over the beam cross-section leads to a remarkable enhancement in the results accuracy. In sharp contrast, a further improvement in the description of bending modes can only be achieved by increasing the number of DOFs in the Ritz expansion.

The possibility to refine separately the displacement components permits to evaluate the effectiveness of certain DOFs leading to a significant reduction of the computational cost. When dealing with both three-dimensional metallic and FG beams, the proposed quasi-3D beam models leads to the same level of accuracy of complex, cumbersome and computationally expensive 3D FEM models.

The proposed results showed also that the dimensionless circular frequency parameters decrease when increasing the p and increase when increasing l/h.

References

[1] L. Euler, De Curvis Elasticis, *Methodus Inveniendi Lineas Curvas Maximi Minimive Proprietate Gaudentes, Sive Solutio Problematis Isoperimetrici Lattissimo Sensu Accepti*, Series 1, Volume 24, Opera Omnia, Bousquet, Geneva, 1744.

[2] S. P. Timoshenko, On the correction for shear of the differential equation for transverse vibrations of prismatic bars, Philosophical Magazine Series 6 (1921) 742–746.

[3] G. R. Cowper, The shear coefficients in timoshenko beam theory, Journal of Applied Mechanics (ASME) 33 (2) (1966) 335–340.

[4] M. Levison, A new rectangular beam theory, Journal of Sound and Vibration, 74 (1) (1981) 81–87.

[5] W. B. Bickford, A consistent higher order beam theory, Dev. in Theoretical and Applied Mechanics, SECTAM 11 (1982) 137–150.

[6] L. W. Rehfield, P. L. N. Murthy, Toward a new new engineering theory of bending: fundamentals, AIAA Journal 20 (5) (1982) 693–699.

[7] A. V. K. Murty, Towards a consistent beam theory, AIAA Journal 22 (6) (1984) 811–816.

[8] A. Bhimaraddi, K. Chandrashekhara, Observations on higher order beam theory, Journal of Aerospace Engineering (ASCE) 6 (4) (1993) 408–413.

[9] W. Yu, D. H. Hodges, Generalized timoshenko theory of the variational asymptotic beam sectional analysis, Journal of the American Helicopter Society 50 (1) (2014) 46–55.

[10] W. Yu, D. H. Hodges, Elasticity solutions versus asymptotic sectional analysis of homogeneous, isotropic, prismatic beams, Journal of Applied Mechanics 71 (1) (2004) 15–23.

[11] W. Yu, V. V. Volvoi, D. H. Hodges, X. Hong, Validation of the variational asymptotic beam sectional analysis, AIAA journal 40 (10) (2002) 2105–2112.

[12] E. Carrera, M. Petrolo, On the effectiveness of higher-order terms in refined beam theories, Journal of Applied Mechanics 78 (2011) 021013–1/021013–17.

[13] A. J. M. Ferreira, G. E. Fasshauer, Computation of natural frequencies of shear deformable beams and plates by an RBF-pseudospectral method, Comput. Methods Appl. Mech. 196 (2006) 134–146.

[14] J. R. Banerjee, Development of an exact dynamic stiffness matrix for free vibration analysis of a twisted timoshenko beam, Journal of Sound and Vibration 270 (1-2) (2004) 379–401.

[15] H. Su, J. R. Banerjee, Development of dynamic stiffness method for the vibration of functionally graded Timoshenko beams, Computers and Structures 147 (2015) 107–116.

[16] H. Su, J. R. Banerjee, C. W. Cheung, Dynamic stiffness formulation and free vibration analysis of functionally graded beams, Computers and Structures 106 (2013) 854–862.

[17] T. P. Vo, H. T. Thai, T. K. Nguyen, Static and vibration analysis of functionally graded beams using refined shear deformation theroy, Meccanica 49 (2014) 155–168.

[18] T. P. Vo, H. T. Thai, T. K. Nguyen, Bending and free vibration of functionally graded beams using various higher-order shear deformation beam theories, International Journal of Mechanical Sciences 62 (1) (2012) 57–66.

[19] M. Simsek, Fundamental frequency analysis of functionally graded beams by using different higher-order beam theories, Nuclear Engineering and Design 240 (4) (2010) 697–705.

[20] M. Simsek, Bi-directional functionally graded materials (BDFGMs) for free and forced vibration of timoshenko beams with various boundary conditions, Composite Structures 133 (2015) 968–978.

[21] X. Chunhua, J.and Wang, Accurate free vibration analysis of Euler functionally graded beams by the weak form quadrature element method, Composites Science and Technology 125 (2015) 41–50.

[22] Z. A. Wang, X. H. Wang, G. D. Xu, S. Cheng, T. Zeng, Free vibration of two-directional functionally graded beams, Composite Structures 135 (2016) 191–198.

[23] C. F. Lü, W. Q. Chen, R. Q. Xu, C. W. Lim, Semi-analytical elasticity solutions for bi-directional functionally graded beams, International Journal of Solids and Structures 45 (1) (2008) 258–275.

[24] A. E. Alshorbagy, M. A. Eltaher, F. F. Mahmoud, Free vibration characteristics of a functionally graded beam by finite element method, Applied Mathematical Modelling 35 (1) (2011) 412–425.

[25] N. V. R. Maganti, M. R. Nullari, Free vibration analysis of pre-twisted rotating FGM beams, International Journal of Mechanics and Materials in Design 9 (4) (2013) 367–383.

[26] N. V. R. Maganti, M. R. Nullari, Flapwise bending vibration analysis of functionally graded rotating double-tapered beams, International Journal of Mechanical and Materials Engineering (2015) 10–21.

[27] S. R. Li, L. L. Fan, Free vibration of FGM Timoshenko beams with through-width delamination, Science China Physics, Mechanics & Astronomy 57 (5) (2014) 927–934.

[28] L. L. Ke, Y. S. Wang, J. Yang, S. Kitipornchai, F. Alam, Nonlinear vibration of edged cracked FGM beams using differential quadrature method, Science China Physics, Mechanics & Astronomy 55 (11) (2012) 2114–2121.

[29] N. Wattanasakulpong, J. Charoensuk, Vibration characteristics of stepped beams made of FGM using differential transformation method, Meccanica 50 (2015) 1089–1101.

[30] N. Wattanasakulpong, A. Chaikittiratana, Flexural vibration of imperfect functionally graded beams based on Timoshenko beam theory: Chebyshev collocation method, Meccanica 50 (2015) 1331–1342.

[31] N. L. Shegokar, A. Lal, Stochastic finite element nonlinear free vibration analysis of piezoelectric functionally graded materials beam subjected to thermo-piezoelectric loadings with material uncertainties, Meccanica 49 (2014) 1039–1068.

[32] A. Shooshtari, M. Rafiee, Nonlinear forced vibration analysis of clamped functionally graded beams, Acta Meccanica 221 (2011) 23–8.

[33] H. Zhu, B. V. Sankar, A combined Fourier series – Galerkin method for the analysis of functionally graded beams, Journal of Applied Mechanics 71 (2004) 421–423.

[34] M. Azadi, Free and forced vibration analysis of FG beam considering temperature dependency of material properties, Journal of Mechanical Science and Technology 25 (1) (2011) 69–80.

[35] K. K. Pradhan, S. Chackraverty, Effects of different shear deformation theories on the free vibration of functionally graded beams, International Journal of Mechanical Sciences 82 (2014) 149–160.

[36] L. Librescu, S. Y. Oh, O. Song, Thin-walled beams made of functionally graded materials and operating in a high temperature environment: Vibration and stability, Journal of Thermal Stresses 28 (2005) 649–712.

[37] G. Giunta, D. Crisafulli, S. Belouettar, E. Carrera, Hierarchical theories for the free vibration analysis of functionally graded beams, Composite Structures 94 (2011) 68–74.

[38] G. Giunta, D. Crisafulli, S. Belouettar, E. Carrera, A thermo-mechanical analysis of functionally graded beams via hierarchical modelling, Composite Structures 95 (2013) 676–690.

[39] N. Zaine, S. A. Meftah, H. A. Belhadj, A. Tounsi, E. A. Bedia, Free vibration analysis of thin and thick-walled FGM box beams, International Journal of Mechanical Sciences 66 (2013) 273–282.

[40] Y. O. Xu, Y. Quian, J. Cheng, G. Song, Stochastic dynamic characteristics of FGM beams with random material properties, Composite Structures 133 (2015) 585–594.

[41] U. Eroglu, In-plane free vibrations of circular beams made of functionally graded material in thermal environment: Beam theory approach, Composite Structures 122 (2015) 217–228.

[42] C. M. C. Roque, P. A. L. S. Martins, Differential evolution for optimization of functionally graded beams, Composite Structures 133 (2015) 1191–1197.

[43] A. Yousefi, A. Rastgoo, Free vibration of functionally graded spatial curved beams, Composite Structures 93 (11) (2011) 3048–3056.

[44] F. Tornabene, 2-D GDQ solution for free vibrations of anisotropic doubly-curved shells and panels of revolution, Composite Structures 93 (2011) 1854–1876.

[45] F. Tornabene, E. Viola, N. Fantuzzi, General higher order equivalent single layer therory for free vibrations of doubly-curved laminated composite shells and panels, Composite Structures 104 (2013) 94–117.

[46] F. Tornabene, Free vibration analysis of functionally graded conical, cylindrical shell and annular plate structures with a four-parameter power-law distribution, Comput. Methods Appl. Mech. Engrg. 198 (2009) 2911–2935.

[47] S. R. Li, R. C. Batra, Relations between buckling loads of functionally graded timoshenko and homogeneous eulerbernoulli beams, Composite Structures 95 (2013) 5–9.

[48] Y. Sun, S. R. Li, R. C. Batra, Thermal buckling and post-buckling of fgm timoshenko beams on nonlinear elastic foundation, Journal of Thermal Stresses 39 (1) (2013) 11–26.

[49] F. A. Fazzolari, E. Carrera, Advanced variable kinematics Ritz and Galerkin formulations for accurate buckling and vibration analysis of laminated composite plates., Composite Structures 94 (1) (2011) 50–67.

[50] F. A. Fazzolari, E. Carrera, Thermo-mechanical buckling analysis of anisotropic multilayered composite and sandwich plates by using refined variable-kinematics theories., Journal of Thermal Stresses, 36 (4) (2012) 321–350.

[51] F. A. Fazzolari, Natural frequencies and critical temperatures of functionally graded sandwich plates subjected to uniform and non-uniform temperature distributions, Composite Structures 121 (2015) 197–210.

[52] F. A. Fazzolari, E. Carrera, Accurate free vibration analysis of thermo-mechanically pre/post-buckled anisotropic multilayered plates based on a refined hierarchical trigonometric Ritz formulation., Composite Structures 95 (2013) 381–402.

[53] F. A. Fazzolari, E. Carrera, Coupled thermoelastic effect in free vibration analysis of anisotropic multilayered plates by using an advanced variable-kinematics Ritz formulation., European Journal of Mechanics Solid/A, 44 (2014) 157–174.

[54] F. A. Fazzolari, E. Carrera, Free vibration analysis of sandwich plates with anisotropic face sheets in thermal environment by using the hierarchical trigonometric Ritz formulation., Composites Part B: Engineering 50 (2013) 67–81.

[55] F. A. Fazzolari, E. Carrera, Advances in the Ritz formulation for free vibration response of doubly-curved anisotropic laminated composite shallow and deep shells., Composite Structures 101 (2013) 111–128.

[56] F. A. Fazzolari, E. Carrera, Thermal stability of FGM sandwich plates under various through-the-thickness temperature distributions, Journal of Thermal Stresses 37 (12) (2014) 1449–1481.

[57] F. A. Fazzolari, J. R. Banerjee, Axiomatic/asymptotic PVD/RMVT-based shell theories for free vibrations of anisotropic shells using an advanced Ritz formulation and accurate curvature descriptions, Composite Structures 108 (2014) 91–110.

[58] F. A. Fazzolari, Reissner's mixed variational theorem and variable kinematics in the modelling of laminated composite and FGM doubly-curved shells, Composites Part B: Engineering 89 (2014) 408–423.

[59] F. A. Fazzolari, Stability analysis of fgm sandwich plates by using variable-kinematics Ritz models, Mechanics of Advanced Materials and Structures 0 (ja) (0) 1–27. doi:10.1080/15376494.2015.1121559.

[60] ABAQUS 6.11 Analysis User's Manual, Dassault Systems, 2011.

[61] ANSYS v10.0 theory manual, ANSYS Inc., Southpointe, PA, 2006.

[62] L. Demasi, ∞^3 hierarchy plate theories for thick and thin composite plate: The Generalized Unified Formulation, Composite Structures 85 (2008) 256–270.

[63] L. Demasi, ∞^6 Mixed plate theories based on the Generalized Unified Formulation. part I: Governing equations, Composite Structures 87 (1) (2009) 1–11.

[64] L. Demasi, ∞^6 Mixed plate theories based on the Generalized Unified Formulation. part III: Advanced mixed higher order shear deformation theories, Composite Structures 87 (3) (2009) 183–194.

[65] E. Carrera, P. Nali, Multilayered plate elements for the analysis of multifield problems, Finite Elements in Analysis and Design 46 (2010) 732–742.

[66] W. Ritz, Über eine neue Methode zur Lösung gewisser Variationsprobleme der mathematischen Physik. (About a new method for the solution of certain variational problems of mathematical physics.), Journal für die Reine und Angewandte Mathematik 135 (1909) 1–61.

[67] J. N. Reddy, Energy Princiles and Variational Methods in Applied Mechanics, 2nd Edition, John Wiley & Sons, Inc., Hoboken, New Jersey, 2002.

[68] J. P. Gram, Üeber die Entwickelung reeller Functionen in Reihen mittelst der Methode der kleinsten Quadrate, Journal für die Reine und Angewandte Mathematik 94 (1883) 41–73.

[69] E. Carrera, F. Miglioretti, M. Petrolo, Computations and evaluations of higher-order theories for free vibration analysis of beams, Journal of Sound and Vibration 331 (9) (2012) 4269–4284.

Tables

Table 1: Taylor's series expansion via Pascal's triangle

N_u	N_u^*	$F_\tau,\ \tau = \tau_x, \tau_y, \tau_z$
0	1	$F_1 = 1$
1	3	$F_2 = x,\ F_3 = y$
2	6	$F_4 = x^2,\ F_5 = x\,y,\ F_6 = y^2$
3	10	$F_7 = x^3,\ F_8 = x^2\,y,\ F_9 = x\,y^2,\ F_{10} = y^3$
$\vdots$	$\vdots$	$\vdots$
N	$\frac{(N+1)(N+2)}{2}$	$F_{\frac{\left(N^2+N+2\right)}{2}} = x^N,\ F_{\frac{\left(N^2+N+4\right)}{2}} = x^{N-1}\,y,\ \cdots\ F_{\frac{N(N+3)}{2}} = x\,y^{N-1},\ F_{\frac{(N+1)(N+2)}{2}} = y^N$

Table 2: Kinematic boundary conditions at the beam ends ($z = 0, l$)

Simply supported (SS)	$u_x = 0,\ u_y = 0$ and $\frac{\partial u_z}{\partial z} = 0$
Clamped (C)	$u_x = 0,\ u_y = 0,\ u_z = 0$ and $\frac{\partial u_z}{\partial z} = 0$
Free (F)	$u_x \neq 0,\ u_y \neq 0$ and $u_z \neq 0$

Table 3: Convergence analysis of the first and seventh natural frequency (Hz) of a cantilever (CF) rectangular metallic beam with $h = 0.1\,m$, $b = 1\,m$ and $l = 10\,m$.

		Hierarchical Beam Theories								
Mode	(i,j)	TE_{222}	TE_{223}	TE_{224}	TE_{422}	TE_{242}	TE_{333}	TE_{444}	TE_{777}	TE_{999}
f_1	4	0.8840	0.8815	0.8815	0.8840	0.8827	0.8815	0.8792	0.8788	0.8788
	6	0.8579	0.8539	0.8539	0.8579	0.8571	0.8539	0.8526	0.8522	0.8522
	8	0.8468	0.8414	0.8414	0.8468	0.8462	0.8415	0.8407	0.8403	0.8403
	10	0.8412	0.8352	0.8352	0.8411	0.8406	0.8352	0.8345	0.8342	0.8342
	12	0.8379	0.8317	0.8317	0.8378	0.8374	0.8317	0.8311	0.8308	0.8308
	14	0.8358	0.8297	0.8297	0.8358	0.8354	0.8297	0.8290	0.8287	0.8287
	16	0.8344	0.8284	0.8284	0.8343	0.8340	0.8284	0.8277	0.8274	0.8274
	18	0.8334	0.8275	0.8275	0.8333	0.8330	0.8275	0.8267	0.8264	0.8264
f_7	4	51.353	51.061	51.061	51.353	51.353	51.061	51.060	51.057	50.985
	6	48.171	48.171	47.648	48.058	48.145	48.030	47.515	47.007	46.799
	8	47.833	47.833	47.315	47.726	47.805	47.698	47.186	46.681	46.476
	10	47.750	47.403	47.232	47.637	47.719	47.403	47.097	46.593	46.388
	12	47.733	47.287	47.216	47.607	47.700	47.287	47.067	46.561	46.357
	14	47.729	47.196	47.196	47.585	47.694	47.196	47.045	46.538	46.333
	16	47.726	47.133	47.133	47.566	47.689	47.133	47.026	46.518	46.312
	18	47.725	47.087	47.087	47.549	47.686	47.087	47.010	46.501	46.297

Table 4: Comparison of the first ten natural frequencies (Hz) of a cantilever (CF) rectangular metallic beam with $h = 0.1\,m$, $b = 1\,m$ and $l = 10\,m$.

	Natural Frequencies										Average
Theory	f_1	f_2	f_3	f_4	f_5	f_6	f_7	f_8	f_9	f_{10}	Rel. Diff(%)
ABAQUS[†]	0.8229	5.1530	8.1179	14.428	15.309	28.286	46.175	46.787	48.665	69.929	
ANSYS[‡]	0.8229	5.1530	8.1179	14.428	15.309	28.286	46.175	46.787	48.665	69.929	(0.00)
TE_{999}	0.8264	5.1748	8.1386	14.489	15.349	28.402	46.297	46.976	48.714	70.205	(0.34)
TE_{888}	0.8264	5.1750	8.1406	14.490	15.349	28.405	46.297	46.981	48.786	70.215	(0.36)
TE_{777}	0.8264	5.1751	8.1406	14.490	15.418	28.405	46.501	46.981	48.786	70.215	(0.45)
TE_{666}	0.8265	5.1758	8.1408	14.492	15.418	28.413	46.503	46.999	48.790	70.250	(0.46)
TE_{555}	0.8266	5.1760	8.1408	14.493	15.580	28.414	46.982	47.002	48.790	70.255	(0.68)
TE_{444}	0.8267	5.1769	8.1413	14.497	15.586	28.423	47.010	47.021	48.794	70.286	(0.71)
TE_{333}	0.8275	5.1817	8.1430	14.511	15.758	28.455	47.087	47.522	48.810	70.416	(1.01)
TE_{242}	0.8330	5.2170	8.1500	14.655	15.787	28.848	47.686	47.872	49.054	71.704	(1.85)
TE_{422}	0.8333	5.2193	8.1507	14.663	15.764	28.866	47.549	47.910	49.059	71.774	(1.84)
TE_{224}	0.8275	5.1817	8.1430	14.511	15.622	28.455	47.087	47.206	48.810	70.416	(0.85)
TE_{223}	0.8275	5.1817	8.1430	14.511	15.795	28.455	47.087	47.725	48.810	70.416	(1.07)
TE_{222}	0.8334	5.2197	8.1507	14.664	15.795	28.870	47.725	47.919	49.059	71.791	(1.91)

[†] 3D FEM, brick element C3DR20 with 20 nodes, mesh $5 \times 10 \times 50$

[‡] 3D FEM, brick element Solid186 with 20 nodes, mesh $5 \times 10 \times 50$

[*] FEM - TE4 (Ref. [69]), $f_1 = 0.8255$, $f_2 = 5.1702$, $f_3 = 8.1443$, $f_4 = 14.479$

Table 5: Comparison of the first ten natural frequencies (Hz) of a CC rectangular metallic beam with $h = 0.1\,m$, $b = 1\,m$ and $l = 10\,m$.

	Natural Frequencies										Average
Theory	f_1	f_2	f_3	f_4	f_5	f_6	f_7	f_8	f_9	f_{10}	Rel. Diff(%)
ABAQUS[†]	5.2669	14.504	28.420	31.470	46.973	48.906	63.481	70.162	96.553	97.972	
TE_{999}	5.3055	14.598	28.622	31.593	47.270	49.009	63.716	70.642	96.940	98.567	(0.54)
TE_{888}	5.3058	14.600	28.625	31.593	47.276	49.118	63.716	70.653	96.941	98.585	(0.57)
TE_{777}	5.3059	14.600	28.625	31.731	47.276	49.118	63.990	70.654	97.348	98.587	(0.70)
TE_{666}	5.3071	14.604	28.635	31.732	47.297	49.126	63.993	70.691	97.354	98.647	(0.73)
TE_{555}	5.3074	14.605	28.637	32.052	47.301	49.126	64.620	70.698	98.264	98.659	(1.03)
TE_{444}	5.3091	14.609	28.648	32.078	47.321	49.136	64.693	70.730	98.425	98.704	(1.09)
TE_{333}	5.3190	14.637	28.704	32.424	47.424	49.165	65.368	70.909	99.001	99.404	(1.55)

[†] 3D FEM, brick element C3DR20 with 20 nodes, mesh $5 \times 10 \times 50$

Table 6: Comparison of the first ten natural frequencies (Hz) of a CS rectangular metallic beam with $h = 0.1\,m$, $b = 1\,m$ and $l = 10\,m$.

	Natural Frequencies										Average
Theory	f_1	f_2	f_3	f_4	f_5	f_6	f_7	f_8	f_9	f_{10}	Rel. Diff(%)
ABAQUS†	3.6068	8.1179	11.689	24.399	30.579	41.754	48.665	61.690	63.759	90.403	
TE_{999}	3.6207	8.1369	11.733	24.491	30.676	41.908	48.706	61.884	63.989	90.722	(0.32)
TE_{888}	3.6209	8.1389	11.734	24.493	30.676	41.913	48.777	61.884	63.999	90.739	(0.34)
TE_{777}	3.6209	8.1390	11.734	24.493	30.812	41.913	48.777	62.154	63.999	90.739	(0.43)
TE_{666}	3.6213	8.1392	11.736	24.500	30.813	41.930	48.781	62.156	64.032	90.795	(0.45)
TE_{555}	3.6215	8.1392	11.736	24.501	31.132	41.932	48.782	62.783	64.035	90.801	(0.66)
TE_{444}	3.6222	8.1397	11.739	24.509	31.146	41.950	48.786	62.833	64.066	90.845	(0.70)
TE_{333}	3.6255	8.1413	11.751	24.536	31.487	42.007	48.801	63.498	64.182	91.062	(1.01)

† 3D FEM, brick element C3DR20 with 20 nodes, mesh $5 \times 10 \times 50$

Table 7: Comparison of the first ten natural frequencies (Hz) of a SS rectangular metallic beam with $h = 0.1\,m$, $b = 1\,m$ and $l = 10\,m$.

	Natural Frequencies										Average
Theory	f_1	f_2	f_3	f_4	f_5	f_6	f_7	f_8	f_9	f_{10}	Rel. Diff(%)
ABAQUS†	2.2932	9.1821	20.690	29.737	36.843	50.202	57.656	59.993	83.126	91.271	
TE_{999}	2.2931	9.1823	20.691	29.817	36.844	50.175	57.658	60.141	83.127	91.506	(0.08)
TE_{888}	2.2932	9.1825	20.692	29.817	36.848	50.201	57.666	60.142	83.141	91.507	(0.08)
TE_{777}	2.2932	9.1825	20.692	29.951	36.848	50.201	57.666	60.409	83.142	91.906	(0.22)
TE_{666}	2.2932	9.1835	20.697	29.952	36.861	50.202	57.694	60.410	83.191	91.908	(0.24)
TE_{555}	2.2932	9.1835	20.697	30.270	36.861	50.202	57.694	61.035	83.192	92.818	(0.55)
TE_{444}	2.2934	9.1850	20.703	30.274	36.877	50.202	57.723	61.063	83.236	92.909	(0.58)
TE_{333}	2.2934	9.1854	20.707	30.610	36.896	50.203	57.783	61.718	83.378	93.854	(0.94)

† 3D FEM, brick element C3DR20 with 20 nodes, mesh $5 \times 10 \times 50$

Table 8: Comparison of the first ten natural frequencies (Hz) of a SF rectangular metallic beam with $h = 0.1\,m$, $b = 1\,m$ and $l = 10\,m$.

	Natural Frequencies										Average
Theory	f_1	f_2	f_3	f_4	f_5	f_6	f_7	f_8	f_9	f_{10}	Rel. Diff(%)
ABAQUS†	3.5823	11.621	14.886	24.279	41.582	44.902	50.202	63.537	75.639	90.138	
TE_{999}	3.5823	11.621	14.914	24.280	41.582	44.985	50.175	63.538	75.776	90.138	(0.06)
TE_{888}	3.5823	11.621	14.914	24.281	41.587	44.985	50.201	63.547	75.776	90.153	(0.06)
TE_{777}	3.5824	11.621	14.981	24.281	41.587	45.187	50.201	63.547	76.112	90.153	(0.20)
TE_{666}	3.5825	11.622	14.981	24.287	41.601	45.187	50.202	63.577	76.113	90.206	(0.21)
TE_{555}	3.5825	11.622	15.143	24.287	41.601	45.665	50.202	63.577	76.889	90.207	(0.53)
TE_{444}	3.5827	11.624	15.143	24.294	41.618	45.677	50.202	63.607	76.944	90.251	(0.56)
TE_{333}	3.5827	11.625	15.313	24.300	41.643	46.181	50.203	63.678	77.764	90.412	(0.93)

† 3D FEM, brick element C3DR20 with 20 nodes, mesh $5 \times 10 \times 50$

Table 9: Comparison of the first ten natural frequencies (Hz) of a FF rectangular metallic beam with $h = 0.1\,m$, $b = 1\,m$ and $l = 10\,m$.

	Natural Frequencies										Average
Theory	f_1	f_2	f_3	f_4	f_5	f_6	f_7	f_8	f_9	f_{10}	Rel. Diff(%)
ABAQUS†	5.1979	14.342	28.153	29.930	46.602	50.202	60.310	69.696	91.570	97.422	
TE_{999}	5.1979	14.342	28.153	29.961	46.602	50.175	60.372	69.695	91.667	97.419	(0.04)
TE_{888}	5.1980	14.343	28.155	29.961	46.606	50.201	60.372	69.705	91.667	97.436	(0.04)
TE_{777}	5.1980	14.343	28.155	30.096	46.606	50.201	60.642	69.705	92.070	97.436	(0.17)
TE_{666}	5.1981	14.345	28.162	30.096	46.623	50.202	60.643	69.737	92.072	97.491	(0.19)
TE_{555}	5.1981	14.345	28.162	30.420	46.623	50.202	61.277	69.738	92.991	97.492	(0.50)
TE_{444}	5.1984	14.347	28.170	30.424	46.641	50.202	61.306	69.768	93.087	97.537	(0.54)
TE_{333}	5.1985	14.348	28.178	30.764	46.672	50.203	61.980	69.852	94.083	97.717	(0.91)

† 3D FEM, brick element C3DR20 with 20 nodes, mesh $5 \times 10 \times 50$

Table 10: First four dimensionless circular frequency parameters of a FG beam with SS boundary condition and volume fraction index $p = 1$.

		Analytical solution, Ref. [37]				Present 3D beam Ritz models			
l/h	Mode	$N = 5$	$N = 4$	$N = 3$	$N = 2$	TE_{555}	TE_{444}	TE_{333}	TE_{222}
5	$\hat{\omega}_1$	14.562	14.563	14.564	14.648	14.562	14.563	14.564	14.648
	$\hat{\omega}_2$	14.726	14.726	14.735	14.827	14.726	14.726	14.735	14.827
	$\hat{\omega}_3$	49.856	49.873	54.117	54.251	49.856	49.873	54.117	54.251
	$\hat{\omega}_4$	85.819	85.819	85.822	85.912	85.819	85.819	85.822	85.912
	Ave. Diff. (%)					(0.00)	(0.00)	(0.00)	(0.00)
10	$\hat{\omega}_1$	3.8026	3.8027	3.8027	3.8099	3.8026	3.8027	3.8027	3.8099
	$\hat{\omega}_2$	3.8568	3.8569	3.8574	3.8656	3.8568	3.8569	3.8574	3.8656
	$\hat{\omega}_3$	24.889	2.4892	27.023	27.091	24.889	2.4892	27.023	27.091
	$\hat{\omega}_4$	43.163	43.163	43.163	43.174	43.163	43.163	43.163	43.174
	Ave. Diff. (%)					(0.00)	(0.00)	(0.00)	(0.00)
100	$\hat{\omega}_1 \times 10^2$	3.8623	3.8624	3.8624	3.8639	3.8623	3.8624	3.8624	3.8639
	$\hat{\omega}_2 \times 10^2$	3.9214	3.9214	3.9214	3.9235	3.9214	3.9214	3.9214	3.9235
	$\hat{\omega}_3$	2.4876	2.4877	2.7011	2.7080	2.4876	2.4877	2.7011	2.7080
	$\hat{\omega}_4$	4.3247	4.3247	4.3247	4.3247	4.3247	4.3247	4.3247	4.3247
	Ave. Diff. (%)					(0.00)	(0.00)	(0.00)	(0.00)

Table 11: Comparison of the first six dimensionless circular frequency parameters of a FG square beam with volume fraction index $p = 1$ and $l/h = 5$.

Boundary		Natural Frequencies						Average
condition	Theory	$\hat{\omega}_1$	$\hat{\omega}_2$	$\hat{\omega}_3$	$\hat{\omega}_4$	$\hat{\omega}_5$	$\hat{\omega}_6$	Rel. Diff(%)
CF	ABAQUS†	4.1108	4.1147	18.605	22.131	22.228	32.713	
	TE_{999}	4.0555	4.0868	18.572	21.628	21.869	32.806	(1.06)
FF	ABAQUS†	7.8757	7.8892	12.313	18.439	18.522	21.570	
	TE_{999}	7.7285	7.7594	12.327	17.695	18.174	21.530	(1.62)

† 3D FEM, brick element C3DR20 with 20 nodes, mesh $10 \times 10 \times 50$

Table 12: First five dimensionless circular frequency parameters of a FG beam with CF boundary condition and $l/h = 5, 20$.

l/h	p		Dimensionless frequency parameters					Ave.	Max.
		Theory	$\hat{\omega}_1$	$\hat{\omega}_2$	$\hat{\omega}_3$	$\hat{\omega}_4$	$\hat{\omega}_5$	Diff(%)	Diff(%)
5	0.1	TBT-DSM[15]	1.7574	9.5011	14.095	22.682	37.747		
		TE_{333}-Ritz	1.7563	9.5203	13.961	22.587	37.563	(0.42)	(0.95)
	0.2	TBT-DSM	1.6638	8.9969	13.390	21.482	35.754		
		TE_{333}-Ritz	1.6486	8.9369	13.344	21.431	35.773	(0.44)	(0.91)
	0.5	TBT-DSM	1.4911	8.0609	12.012	19.243	32.022		
		TE_{333}-Ritz	1.4869	8.0470	12.071	19.190	32.190	(0.35)	(0.52)
	1	TBT-DSM	1.3557	7.3164	10.811	17.441	28.989		
		TE_{333}-Ritz	1.3490	7.2760	10.905	17.430	29.024	(0.42)	(0.87)
	2	TBT-DSM	1.2471	6.7053	9.7403	15.937	26.428		
		TE_{333}-Ritz	1.2389	6.6425	9.8351	15.847	26.312	(0.71)	(0.97)
	5	TBT-DSM	1.1446	6.1274	8.7633	14.516	24.009		
		TE_{333}-Ritz	1.1467	6.1104	8.8486	14.490	23.975	(0.35)	(0.97)
	10	TBT-DSM	1.0867	5.8159	8.3430	13.776	22.783		
		TE_{333}-Ritz	1.0989	5.8613	8.4308	13.890	22.990	(0.94)	(1.12)
20	0.1	TBT-DSM[15]	1.8070	11.196	30.800	56.379	58.897		
		TE_{333}-Ritz	1.7971	11.135	30.630	55.644	58.579	(0.70)	(1.30)
	0.2	TBT-DSM	1.7107	10.600	29.161	53.562	55.762		
		TE_{333}-Ritz	1.6859	10.448	28.759	53.139	55.932	(1.07)	(1.50)
	0.5	TBT-DSM	1.5332	9.4992	26.130	48.048	49.962		
		TE_{333}-Ritz	1.5202	9.4205	25.928	47.967	49.692	(0.63)	(0.85)
	1	TBT-DSM	1.3945	8.6383	23.755	43.246	45.402		
		TE_{333}-Ritz	1.3995	8.6656	23.812	43.268	45.505	(0.24)	(0.36)
	2	TBT-DSM	1.2839	7.9501	21.851	38.961	41.733		
		TE_{333}-Ritz	1.2682	7.8529	21.586	39.032	41.299	(0.98)	(1.22)
	5	TBT-DSM	1.1795	7.3014	20.057	35.053	38.278		
		TE_{333}-Ritz	1.1754	7.2729	19.971	35.182	38.124	(0.39)	(0.43)
	10	TBT-DSM	1.1199	6.9324	19.043	33.372	36.345		
		TE_{333}-Ritz	1.1261	6.9685	19.136	33.557	36.520	(0.52)	(0.55)

Table 13: First five dimensionless circular frequency parameters of a FG beam with CC boundary condition and $l/h = 5, 20$.

l/h	p		Dimensionless frequency parameters					Ave.	Max.
		Theory	$\hat{\omega}_1$	$\hat{\omega}_2$	$\hat{\omega}_3$	$\hat{\omega}_4$	$\hat{\omega}_5$	Diff(%)	Diff(%)
5	0.1	TBT-DSM[15]	9.3380	21.455	28.189	35.825	51.248		
		TE_{333}-Ritz	9.3109	21.475	27.985	35.839	51.173	(0.26)	(0.72)
	0.2	TBT-DSM	8.8467	20.331	26.780	33.952	48.571		
		TE_{333}-Ritz	8.8841	20.449	26.721	34.034	48.475	(0.33)	(0.58)
	0.5	TBT-DSM	7.9241	18.206	24.022	30.399	43.484		
		TE_{333}-Ritz	8.0119	18.295	24.106	30.317	42.955	(0.69)	(1.22)
	1	TBT-DSM	7.1772	16.459	21.621	27.456	39.251		
		TE_{333}-Ritz	7.2046	16.392	21.728	27.549	39.777	(0.59)	(1.34)
	2	TBT-DSM	6.5543	14.974	19.479	24.932	35.603		
		TE_{333}-Ritz	6.5857	15.044	19.594	25.108	35.871	(0.60)	(0.75)
	5	TBT-DSM	5.9699	13.585	17.526	22.573	32.193		
		TE_{333}-Ritz	6.0163	13.662	17.694	22.742	32.466	(0.78)	(0.96)
	10	TBT-DSM	5.6680	12.896	16.686	21.428	30.559		
		TE_{333}-Ritz	5.6431	12.904	16.904	21.493	30.684	(0.50)	(1.31)
20	0.1	TBT-DSM[15]	11.334	30.602	58.430	93.607	112.76		
		TE_{333}-Ritz	11.299	30.498	58.220	93.264	111.46	(0.51)	(1.15)
	0.2	TBT-DSM	10.731	28.974	55.324	88.635	107.12		
		TE_{333}-Ritz	10.614	28.669	55.574	87.888	106.47	(0.81)	(1.09)
	0.5	TBT-DSM	9.6159	25.961	49.565	79.395	96.090		
		TE_{333}-Ritz	9.5725	25.853	49.423	79.233	96.177	(0.29)	(0.45)
	1	TBT-DSM	8.7425	23.593	45.019	72.072	86.486		
		TE_{333}-Ritz	8.6856	23.445	45.156	72.273	86.783	(0.44)	(0.65)
	2	TBT-DSM	8.0431	21.688	41.347	66.128	77.917		
		TE_{333}-Ritz	7.9780	21.509	41.040	65.651	78.255	(0.71)	(0.83)
	5	TBT-DSM	7.3844	19.896	37.898	60.554	70.104		
		TE_{333}-Ritz	7.3849	19.880	37.867	60.464	70.507	(0.18)	(0.57)
	10	TBT-DSM	7.0116	18.892	35.987	57.504	66.743		
		TE_{333}-Ritz	7.0761	19.048	36.283	57.935	67.247	(0.81)	(0.92)

Table 14: First five dimensionless circular frequency parameters of a FG beam with CS boundary condition and $l/h = 5, 20$.

l/h	p		Dimensionless frequency parameters					Ave.	Max.
		Theory	$\hat{\omega}_1$	$\hat{\omega}_2$	$\hat{\omega}_3$	$\hat{\omega}_4$	$\hat{\omega}_5$	Diff(%)	Diff(%)
5	0.1	TBT-DSM[15]	6.9523	19.153	28.189	33.951	49.968		
		TE_{333}-Ritz	6.9422	19.130	27.985	33.829	49.938	(0.28)	(0.72)
	0.2	TBT-DSM	6.5845	18.144	26.780	32.169	47.351		
		TE_{333}-Ritz	6.5494	18.132	26.721	32.052	47.095	(0.34)	(0.54)
	0.5	TBT-DSM	5.8992	16.252	24.022	28.807	42.396		
		TE_{333}-Ritz	5.9046	16.339	24.106	28.582	42.836	(0.56)	(1.04)
	1	TBT-DSM	5.3522	14.717	21.621	26.051	38.300		
		TE_{333}-Ritz	5.3439	14.752	21.728	26.182	38.567	(0.42)	(0.70)
	2	TBT-DSM	4.9032	13.431	19.479	23.711	34.791		
		TE_{333}-Ritz	4.8783	13.393	19.594	23.688	34.829	(0.32)	(0.59)
	5	TBT-DSM	4.4805	12.222	17.526	21.514	31.503		
		TE_{333}-Ritz	4.4800	12.214	17.694	21.518	31.565	(0.25)	(0.96)
	10	TBT-DSM	4.2537	11.602	16.686	20.422	29.903		
		TE_{333}-Ritz	4.2923	11.515	16.904	20.298	29.837	(0.76)	(1.31)
20	0.1	TBT-DSM[15]	7.8636	25.073	51.128	84.981	112.76		
		TE_{333}-Ritz	7.8192	24.931	50.838	84.511	111.46	(0.68)	(1.15)
	0.2	TBT-DSM	7.4449	23.739	48.408	80.462	107.12		
		TE_{333}-Ritz	7.4688	23.810	48.540	80.674	106.47	(0.35)	(0.61)
	0.5	TBT-DSM	6.6719	21.272	43.373	72.083	96.090		
		TE_{333}-Ritz	6.6156	21.106	43.073	71.669	96.177	(0.60)	(0.84)
	1	TBT-DSM	6.0672	19.337	39.412	65.467	86.486		
		TE_{333}-Ritz	6.0863	19.389	39.485	65.568	86.783	(0.25)	(0.34)
	2	TBT-DSM	5.5838	17.787	36.223	60.118	77.917		
		TE_{333}-Ritz	5.5151	17.572	35.802	59.459	78.255	(1.03)	(1.23)
	5	TBT-DSM	5.1283	16.326	33.224	55.092	70.104		
		TE_{333}-Ritz	5.1078	16.256	33.072	54.833	70.507	(0.47)	(0.57)
	10	TBT-DSM	4.8692	15.502	31.547	52.314	66.743		
		TE_{333}-Ritz	4.8937	15.574	31.688	52.537	67.247	(0.52)	(0.76)

Figures

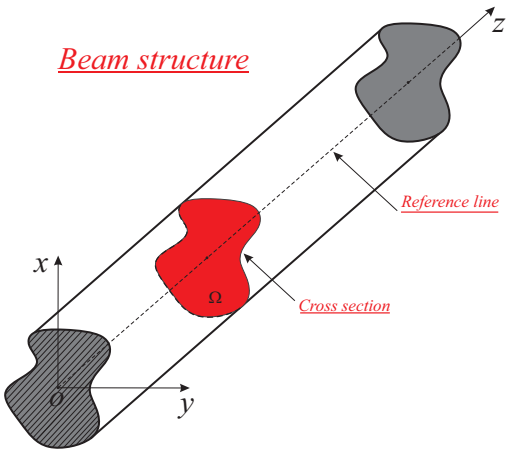

Figure 1: Beam structure and coordinate system.

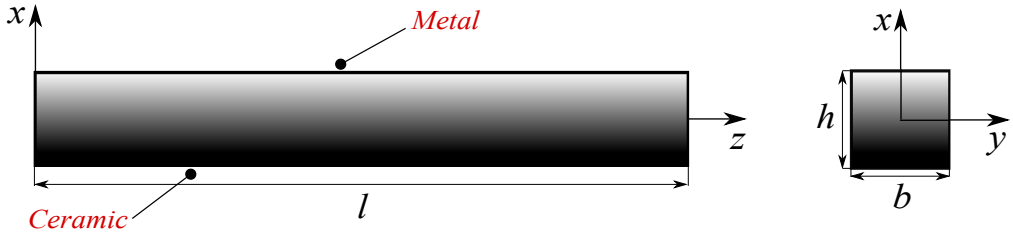

Figure 2: FG beam structure.

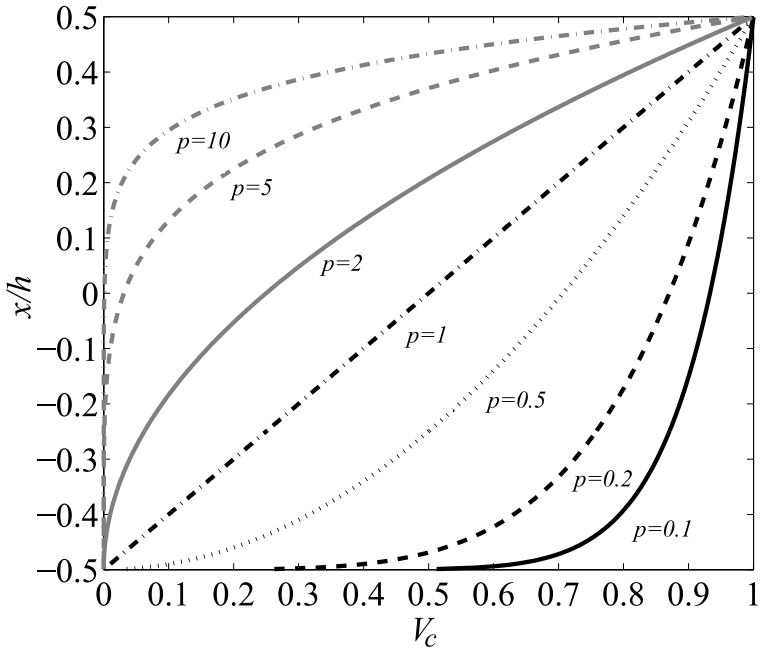

Figure 3: Volume fraction of the ceramic constituent.

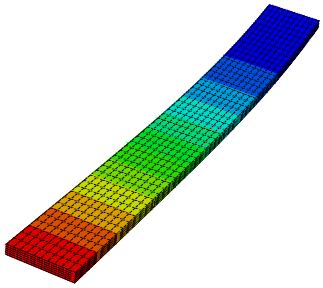

(a) f_1, Bending mode (xz)

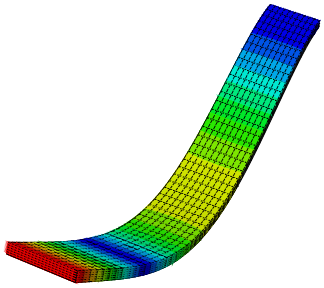

(b) f_2, Bending mode (xz)

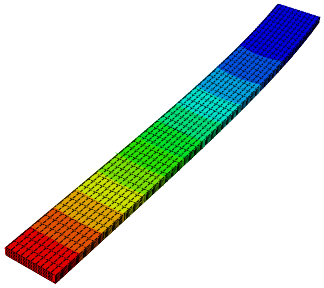

(c) f_3, Bending mode (yz)

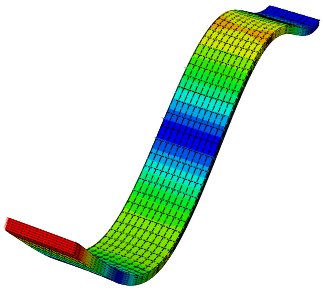

(d) f_4, Bending mode (xz)

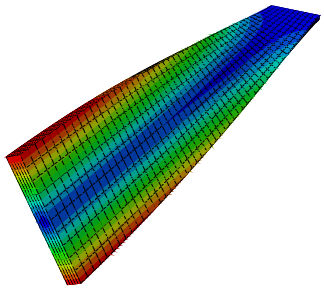

(e) f_5, Torsional mode

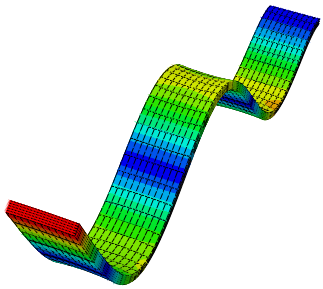

(f) f_6, Bending mode (xz)

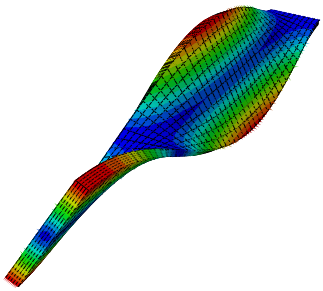

(g) f_7, Torsional mode

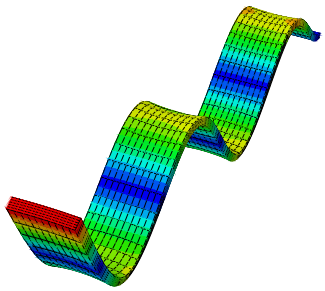

(h) f_8, Bending mode (xz)

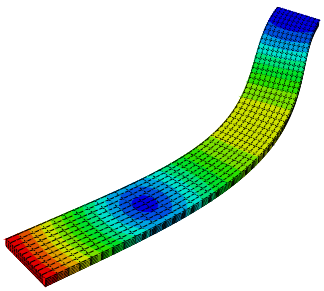

(i) f_9, Bending mode (yz)

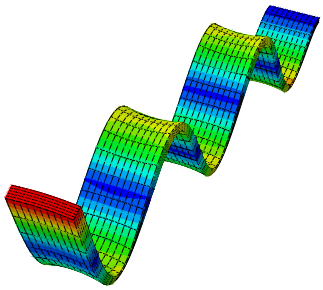

(j) f_{10}, Bending mode (xz)

Figure 4: First 10 mode shapes of a rectangular metal beam with CF boundary condition, $l/b = 10$ and $b/h = 10$.

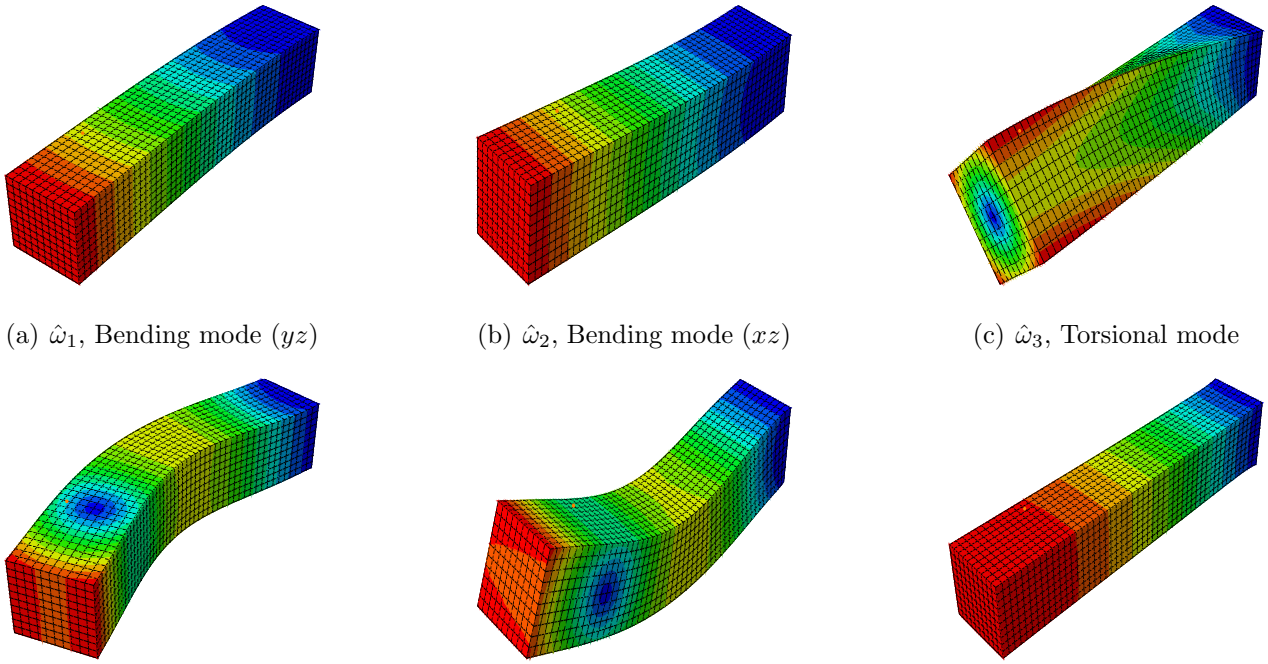

(a) $\hat{\omega}_1$, Bending mode (yz) (b) $\hat{\omega}_2$, Bending mode (xz) (c) $\hat{\omega}_3$, Torsional mode

(d) $\hat{\omega}_4$, Bending mode (yz) (e) $\hat{\omega}_5$, Bending mode (xz) (f) $\hat{\omega}_6$, Axial mode

Figure 5: The first 6 mode shapes of a square FG beam with CF boundary condition and $l/h = 5$.

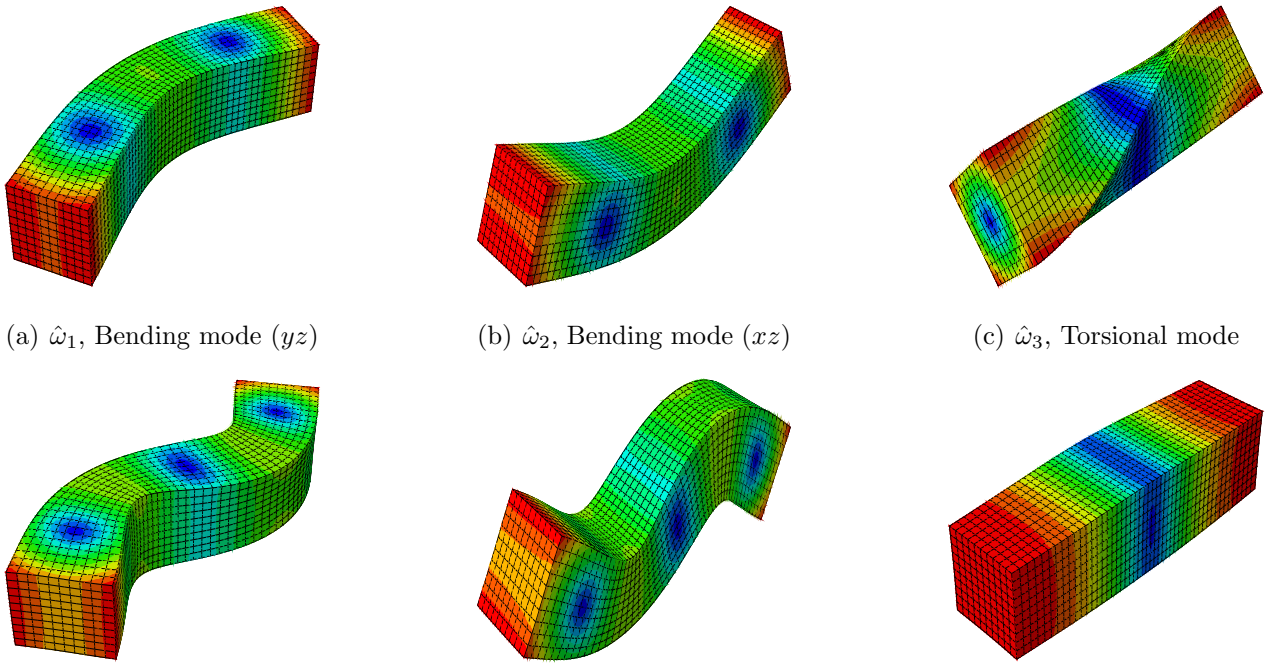

(a) $\hat{\omega}_1$, Bending mode (yz) (b) $\hat{\omega}_2$, Bending mode (xz) (c) $\hat{\omega}_3$, Torsional mode

(d) $\hat{\omega}_4$, Bending mode (yz) (e) $\hat{\omega}_5$, Bending mode (xz) (f) $\hat{\omega}_6$, Axial mode

Figure 6: The first 6 mode shapes of a square FG beam with FF boundary condition and $l/h = 5$.